Photoluminescence of InN with Mg and Zn Dopants

A thesis
submitted in partial fulfilment
of the requirements for the Degree
of
Master of Science in Physics
in the
University of Canterbury
by
Young Wook Song

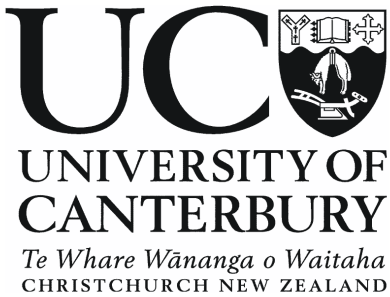

University of Canterbury
2008

Abstract

The optical properties of Mg-doped InN thin films grown on YSZ substrates have been investigated by photoluminescence (PL). A series of InN:Mg samples with various Mg cell temperatures (T_{Mg}) were produced by molecular beam epitaxy. The effect of Mg concentration on PL emission properties have been explored by various excitation power and temperature dependent measurements. The PL spectra as a function of excitation power exhibited a pronounce blueshift, indicating prominent band filling caused by the Burstein-Moss effect. Meanwhile, a typical redshift was observed as temperature increased due to bandgap shrinkage. The samples with T_{Mg} below 210 ˚C have a dominant peak at energy of 0.68 eV. In contrast, the PL peak emissions for films with a high T_{Mg} between 210~230 ˚C were centred near 0.6 eV. No PL emission was observed from the films with T_{Mg} above 230 ˚C. By fitting with an empirical Arrhenius equation, the activation energies yield approximately 20 meV and 15 meV for the lower and higher energy transitions, respectively.

The fundamental optical properties of Zn doped InN were also examined. InN:Zn films were grown under In-rich conditions. The samples showed well defined PL emission spectra implying that the quality of the film has been improved over the Mg-doped series. The PL spectra of InN:Zn exhibited prominent features containing various emission peaks. The combination of excitation power and temperature dependent measurements supports a precise determination for the origins of the observed transitions. The comparison between the optical properties of Mg and Zn doped InN provide the motivation for more precise quantitative interpretation of p-type InN.

Acknowledgement

Fist of all, I would like to thank my supervisor Assoc. Prof. Roger Reeves for his patient guidance, huge support and encouragement throughout all stages of this work. I also would like to thank to Dr Steve Durbin for his invaluable advice and constant enthusiasm towards the topic.

During course of this work, Russell Gillard has provided many litres of liquid Helium for the experimental work which has been greatly appreciated. I am grateful to Wayne Smith and Ross Ritchie for their excellent assistance at providing the technical support.

FTIR measurements were performed with the assistance of Dr Glynn Jones and Dr Jon-Paul Wells, whose contributions were much appreciated.

Film growths and Hall measurements were largely taken by Chito Kendrick and Craig Swartz from Electrical Engineering, to whom I am each very thankful. Also, many thanks to my fellow research students, Ian Farrell, Martin Henseler, Adam Hyndman and Paul Miller who made the student life enjoyable. And special thanks to Rueben Mendelsberg and Scott Choi for many helpful discussions and assistance in the operation of the laser laboratory. Finally, I thank the Department of Physics and Astronomy for the opportunity to work here.

Last but not least, I would like to thank my parents and Hyun-Jung for their endless love and great encouragement throughout the year.

Contents

Figures

Tables

Chapter 1 Introduction

1.1 Introduction to InN

Indium Nitride (InN) is a group III-V semiconductor that is part of the Al, Ga, In:N family. The optical properties of GaN are well known as this semiconductor forms the basis of "blue" light emitting devices through its bandgap of ~3.5 eV. AlN has a bandgap of around 6 eV and when alloyed with GaN, the AlGaN family can span the blue to ultraviolet region. In contrast, InN is narrow bandgap semiconductor and its fundamental properties are much less known. In the early days, research interest was concentrated on GaN or Ga-rich InGaN, which are efficient light emitters even with relatively high defect concentrations [1]. InN was believed to be a poor emitter and the fundamental bandgap energy was anomalous due to the difficulty in producing high quality samples [2].

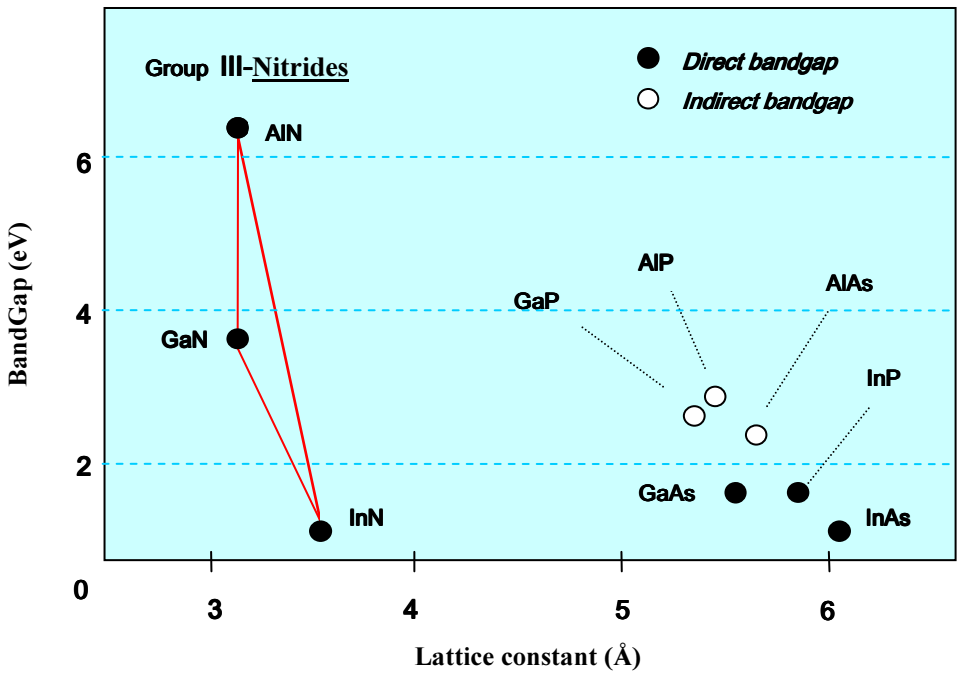

Fig. 1.1 Bandgap of group III-nitride semiconductors as a function of the lattice constant. The materials included in the diagram are the ones commonly used for making LEDs and laser diodes.

The first report on InN was in 1938 by Juza *et al.* who synthesized GaN and InN crystallites with InF_6 $(NH_4)_3$ reductions. In 1985, Foley and Tansley [3] reported the fundamental bandgap of InN to be 1.9 eV by investigating optical absorption spectra and the interest in InN was restricted to its role as a binary endpoint of InGaN alloys for a few decades. However, in 2001 Davydov *et al*. introduced plausible evidence that the bandgap of InN was below 1 eV by using the molecular beam epitaxy (MBE) growth technique and photoluminescence (PL) characterization. Subsequently, many research groups have confirmed the bandgap energy of InN is within the infrared region ~0.7 eV by investigating samples grown by techniques such as MBE and MOCVD (metal organic chemical vapour deposition). However, there has still been a heated debate over the past few years regarding InN's bandgap. The main contention was that in previous reports the films were grown with a relatively high concentration of oxygen defects and bandgap determination was mostly based on optical absorption [2].

The prospect of a bandgap near 0.7 eV provides considerable motivation towards nitride based pn junctions spanning the entire visible spectrum, from the near infrared to the ultraviolet. Despite significant research on group III -nitrides, InN is still studied much less in contrast to matured semiconductors such as GaN. Since the comprehensive study on fundamental properties of InN was commenced after Davydov's work in 2001, the growth of high quality films and determining their optical properties still remains a formidable challenge. The main hurdles to cross are its stoichiometric instability and low dissociation temperature [4].

However, since the new bandgap was determined, InN becomes an attractive candidate for nitride based semiconductors and its development is progressing at a remarkable rate. Thus, InN has received significant attention in recent years due to its potential applications for various optoelectronic devices such as solar cells and optical coatings [5]. During the last few years a large number of papers devoted to the growth and characterization of InN have been published [1~6, 8~12]. The development of a wide range of $In_xGa_{1-x}N$ alloy based light emitting diodes (LEDs) from red to blue and even white means III -nitrides (GaN, AlN and InN) are the most important semiconductors since silicon. The performance and efficiency of nitride-based LEDs have been continuously improving in the past decades. In addition, nitride based high electron mobility transistors (HEMTs) have become promising candidates for high frequency and high power applications in the future [14].

1.2 Growth and Sample Preparation

The leading modern technique for high quality InN film growth is molecular beam epitaxy (MBE). The term, "molecular beam" itself is defined as 'a directed ray of neutral molecules or atoms in a vacuum system' [7]. The samples used in this study were grown at the Electrical and Computer Engineering Department, University of Canterbury using a Perkin-Elmer 430 MBE system. Since the crucial aspect to minimize impurities is to maintain the vacuum during growth, the whole system operates at a pressure of ~10^{-10} torr.

The substrate is mounted in a load lock and baked at 100 ˚C to prevent any water vapour entering the system. Then the substrate plate is shifted inside the main growth chamber by a transfer tube. Active nitrogen is supplied by an RF plasma source and all metallic species such as indium, are produced by standard effusion cells. The growth procedure can be monitored by a Staib Instrument reflection high energy electron diffraction (RHEED) system.

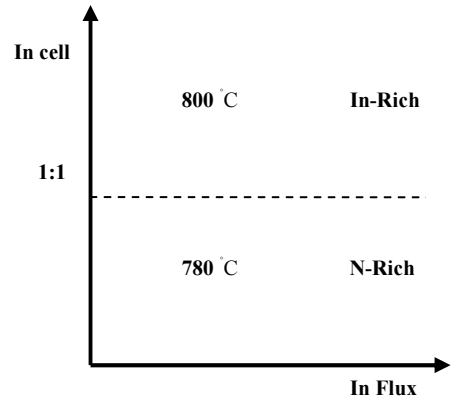

Figure 1.2 The schematic diagram for growth with various In flux. Most samples in this research have been grown under the N-rich condition. Both conditions can be regulated by the In cell temperature. For N-rich growth, the In cell temperature needed to be under 780 ˚C. For In-rich condition, the In cell temperature should reach 800 ˚C or more

In this research, magnesium, zinc and calcium have been chosen as potential p-type dopants for InN. Thirty five doped InN samples have been studied. The list of samples is displayed in table 1.1 showing dopants and substrates. For Zn doped InN, growth was completed under both In and N-rich circumstances. The major benefit of growth under In-rich condition is the completion of a monolayer on the substrate. However, In accumulation during growth may affect the properties of the samples.

Table 1.1. The list of samples with indication of dopants and substrates, produced by Electrical and Computer Engineering Department.

Sample	Substrate	PL	Sample	Substrate	PL
222-InN:Ca	Sapphire	No	604-InN:Zn	YSZ(111)	No
227-InN:Ca	Sapphire	No	610-InN:Zn	YSZ(111)	No
288-InN:Ca	Sapphire	Yes	611-InN:Zn	YSZ(111)	No
325-InN:Ca	Sapphire	Yes	612-InN:Zn	YSZ(111)	No
554-InN:Mg	YSZ(111)	No	613-InN:Zn	YSZ(111)	Yes
555-InN:Mg	YSZ(111)	Yes	615-InN:Zn	YSZ(111)	No
557-InN:Mg	YSZ(111)	No	617-InN:Zn	YSZ(111)	No
577-InN:Mg	YSZ(111)	Yes	619-InN:Zn	MOCVD GaN	No
579-InN:Mg	YSZ(111)	Yes	621-InN:Zn	MOCVD GaN	No
580-InN:Mg	YSZ(111)	No	627-InN:Zn	MOCVD GaN	Yes
583-InN:Mg	YSZ(111)	No	634-InN:Zn	YSZ(111)	Yes
584-InN:Mg	YSZ(111)	No	637-InN*	YSZ(111)	Yes
585-InN:Mg	YSZ(111)	Yes	649-InGaN:Zn*	MOCVD GaN	No
590-InN:Mg	YSZ(111)	Yes	651-InGaN:Zn*	MOCVD GaN	No
591-InN:Mg	MOCVD GaN	No	652-InGaN:Zn*	MOCVD GaN	No
594-InN:Mg	YSZ(111)	Yes	653-InN:Zn*	MOCVD GaN	Yes
598-InN:Mg	MOCVD GaN	No	655-InN:Zn*	MOCVD GaN	Yes
601-InN:Mg	YSZ(111)	Yes	656-InN:Zn*	MOCVD GaN	Yes

Note: The sample numbers with * were grown under In-Rich conditions.

YSZ - Yttrium Stabilized Zirconia

MOCVD - Metal Organic Chemical Vapour Deposition.

1.3 Mg doped InN

Ever since InN was confirmed to be a narrow band gap semiconductor with a band gap energy of about 0.7 eV [8-11], growing p-type doped InN has gained attention in order to fabricate pn junctions. Nitride devices are typically based on $In_xGa_{1-x}N$ [9], which has intensified investigation into the fundamental properties of p-type InN. Magnesium (Mg) is expected to be the most suitable candidate for p-type due to its similar atomic radius with indium (Mg~159.9pm and In~162.6pm). Khan *at al*. suggested that Mg atoms occupy either the In metal (Mg_{In}) or the interstitial (Mg_i) based on x-ray absorption fine structure analysis [10]. Also recently Anderson *et al*. reported a combination of capacitance-voltage (CV) and photoluminescence (PL) data which accounted for the effect of the surface charge layer and provided the first indirect evidence for buried p-type layers in Mg doped InN thin films [11]. In addition, the great success in establishing Mg doped GaN and AlN, has provided potential motivation to achieve p-type InN [12]. Since, very few studies have been done on the basic properties of Mg-doped InN [13], many aspects of luminescence mechanisms are unknown.

In this thesis, the optical properties of p-type InN will be discussed based on direct evidence from laser spectroscopy. Considering the similarity between InN and GaN, Mg is chosen to be the first candidate for viable p-type dopant of InN. A series of Mg doped InN samples have been examined under various circumstances and Mg dopability of InN is investigated. The general aim of this research is focused on characterizing the optical properties of p-type doped InN by using PL. The results of this study may provide a significant step towards fabrication of InN pn junction devices.

1.4. Outline

As is mentioned in a previous section, the main purpose of this research is investigating the Mg dopability and its optical properties of InN. Eventually, Zn is also briefly introduced as a potential p-type dopant and the combination of both dopants will support the comprehensive study of p-type InN.

In chapter two, the important theoretical review of PL and its major processes will be discussed to assist understanding the optical properties of p-type InN. Also the major role of each component in the experimental set up will be mentioned.

In chapter three, the results of PL for Mg doped InN is discussed. To evaluate the Mg dopability of InN, a series of InN:Mg samples from Mg cell temperature 170 to 370 ˚C have been analyzed by SIMS (secondary ion mass spectroscopy). Effects of the Mg concentration on PL emission properties of Mg doped InN has been studied. Eventually, the optical properties of each sample have been examined under excitation power and temperature variations.

In chapter four, Zn is introduced as another consideration for a potential dopant for InN. Two different growth methods, N-rich and In-rich are examined by using PL. The plausible PL emissions are determined and their optical properties are characterized by detailed plots.

Finally, the general overview of the PL results is discussed in chapter five. The comparison between optical characterization for both Mg and Zn doped are determined and future prospect for p-type dopant of InN is briefly mentioned. For the further work of this research, the new combination of spectrometer and detector is suggested and their prominent PL results are introduced.

1.5 References

[1] W. Walukiewicz, S.X. Li, J. Wu, K.M. Yu, J.W. Ager III, E.E. Haller, Hai Lu, William J. Schaff, Journal of Crystal Growth **269** (2004) 119-127

[2] C. Hsiao, H. Hsu, L. Chen, C. Wu, C. Chen, M. Chen, L. Tu and K, Chen, Appl. Phys. Lett. **91**, 181912 (2007)

[3] C. Foley, T. Tansley, Appl. Surface. Sci, Vol **22-3**, 663-669 (1985)

[4] S. Z. Wang, S. F. Yoon, Y. X. Xia, S. W. Xie, Journal of Appl. Phys Vol **95**, No. 12 (2004)

[5] S.Strite, H. Morkoc, J. Vac. Sci. Technol. **B** 10 (1992) 1237

[6] B. Arnaudov, T. Paskova, P. P. Paskov, B. Magusson, E. Valcheva, and B. Monemar, H. Lu, W. J. Schaff, H. Amano and I. Akasaki, Phys Review B **69**, 115216 (2004)

[7] J.G Choi 2004 *Laser spectroscopy of* Eu^{3+} *ions in* CaF_2/CdF_2 *super-lattices* Masters Thesis (University of Canterbury)

[8] J.Wu, W. Walukiewicz, K.M. Yu, J.W. Ager, E. E. Haller, H. Lu, W. J. Schaff, Y. Saito, and Y. Nanishi, Appl. Phys. Lett. **80,** 3967 (2002)

[9] W. Walukiewicz, S.X. Li, J. Wu, K.M. Yu, J.W. Ager III, E.E. Haller, Hai Lu, William J. Schaff, Journal of Crystal Growth **269** (2004) 119-127

[10] N. Khan, N. Nepal, A. Sedhain, J. Y. Lin, and H. X. Jiang, Appl. Phys. Lett. **91**, 012101 (2007)

[11] P.A. Anderson, C.H. Swartz, D. Carder, R. J. Reeves, and S. M. Durbin. Appl Phys Lett 89 184104 (2006)

[12] S. M. Durbin, C. E. Kendrick, C.H. Swartz, Y. W. Song, R. J. Reeves, J. Kennedy, Abstract for in 7th Nitride Conference. Las Vegas, USA (2007).

[13] V. V. Mamutin, V.A. Vekshin, V. Yu. Davydov, V. V. Ratnikov, Yu. A. Kudriavtsev, B. Ya. Ber, V. V. Emtsev, and S. V. Ivanov, Phys. Status Solidi A **176**, 373 (1999)

[14] P. A. Anderson 2006 *Indium Nitride: An Investigtion of growth, electronic structure and doping* Ph.D Thesis (University of Canterbury)

Chapter 2 Optical Processes in Semiconductors and Experimental Details

2.1 The band theory

The major electronic aspects of a solid are determined by the spacing between the electron bands, by the occupation of the bands, and by the relative location of the Fermi energy. In this section, these three aspects of band theory will be briefly introduced.

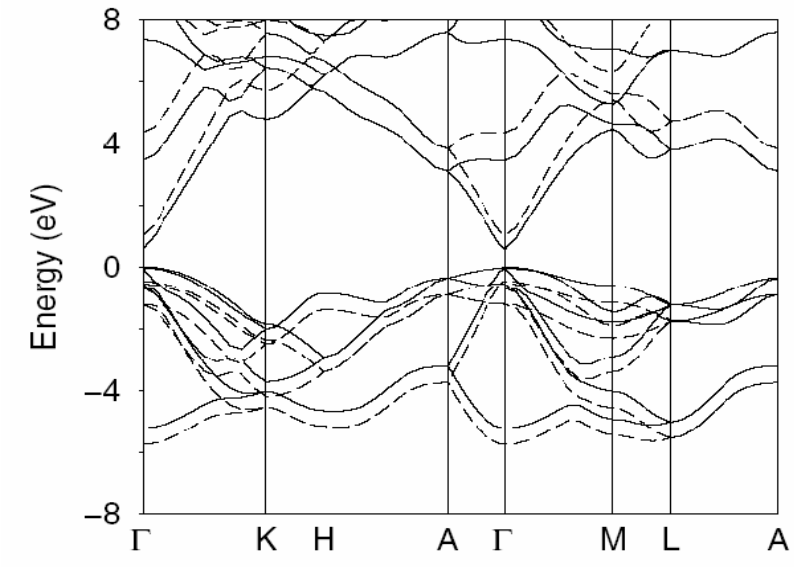

Figure 2.1 Energy Band structure of wurtzite InN: Solid lines: DFT-LDA, dashed lines: including quasiparticle corrections [Bechstedt *et* al Phys. Stat. Sol. (a), 195 (2003) 628]

Band Structure - As it discussed in previous chapter, the optical bandgap of InN has been the issue of much debate over last few years [1,6,7,8]. The bandgap is defined to be the minimum energy between the valence band maximum and conduction band minimum. There are two types of bandgap structures: direct and indirect gap. The distinction concerns the relative positions of the two bands (valence band maximum and conduction band minimum)

in the Brillouin zone. In a direct bandgap material, these extrema occur at the zone center, k=0 where k is the electron momentum. Meanwhile, the conduction band minimum occurs at some other values of k for an indirect bandgap [3].

The shape of the band structure and its characteristics can be predicted by using theoretical techniques [1]. Figure 2.1 depicts the energy band structure around 1st Brillouin zone of wurtzite InN by using DFT* and LDA** methods. This calculation clearly describes InN is a direct bandgap semiconductor by showing the valence band maximum and conduction band minimum lying at the same wave vector Γ. Since InN is the direct gap semiconductor, it has no separation in momentum space between the two bands extrema. This allows an electric dipole transition and the electrons and holes can recombine across the bandgap without requiring a phonon to participate [2,3].

Fermi-Dirac statistics - Evaluating the occupancy probability for electrons in conduction band is another crucial strategy to understand the general properties of semiconductor. In fact, the electrons contribute to the conductivity of semiconductor only if there is an occupying state available for electrons in the conduction band. In order to calculate the properties at temperature above absolute zero (T > 0 K), the description of the thermal occupation of the allowed quantum states is required [4]. Thus the electron distribution can be specifically described by a set of quantum counting rules called Fermi-Dirac statistics. It can be determined by the equation

$$N_e = \int_{E_g}^{\infty} g_c(E) f_e(E) dE \tag{2.1}$$

where

$$g_c(E) = \frac{1}{2\pi^2}\left(\frac{2m_e^*}{\hbar^2}\right)^{\frac{3}{2}}\left(E - E_g\right)^{\frac{1}{2}}, \text{ and } \quad f_e(E) = \left[\exp\left(\frac{E - E_F^c}{k_B T}\right) + 1\right]^{-1} \tag{2.2}$$

N_e represents the total number density of electrons in the conduction band governed by the functions, the density of states, and Fermi-Dirac distributions $f_e(E)$. It is important to realize

---

* Density Functional Theory

** Local Density Approximation

when statistical mechanics are applied the system is in a non-equilibrium situation [3]. Since there are thermal excitations of electrons across the bandgap, there are a large numbers of electrons and holes activating.

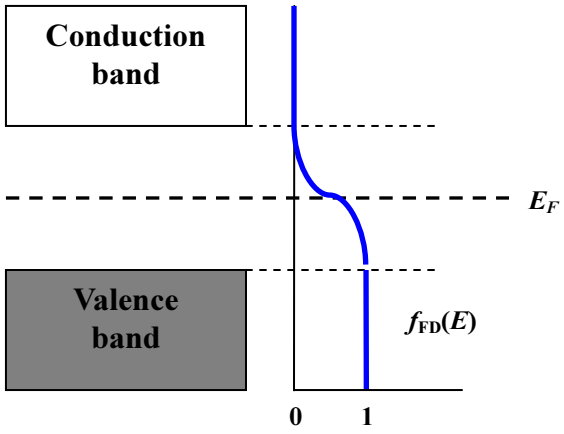

Figure 2.2 Band structure of a semiconductor (intrinsic) with schematic of Fermi-Dirac distribution on the right, where E_F represents Fermi energy in pure semiconductor at T >0. The energy of which the probability of occupancy is one half is E_F, the Fermi energy.

It is worth noting that the Fermi-Dirac distribution does not depend on the energy E of the level but only on the difference E-E_F. The Fermi energy (E_F) as displayed in figure 2.2 can be changed by adding impurities in very low concentration. This process is known as doping and can have a great effect on the conductivity and can also change the optical characteristics of the semiconductor. In contrast to insulators and conductors, thermal excitation across the gap is relatively probable for semiconductors causing the electrical conductivity of semiconductors to be strongly dependent on temperature [5].

2.2 Optical Absorption

2.2.1 Direct and Indirect Bandgap

Over the last few decades optical properties of semiconductors have been comprehensively investigated [6,7,8]. For example, the optical absorption is widely used to determine the bandgap and thus contribute to understanding the fundamental properties of semiconductors. Also the understanding of optical absorption motivates significant steps towards the luminescence mechanisms. The general aspect of interband optical absorption in doped semiconductors can be described as the transitions from populated states of the valence band to unpopulated states of the conduction band [5]. Therefore, measuring the optical absorption of a material by applying different photon energy provides an illustration of possible transitions.

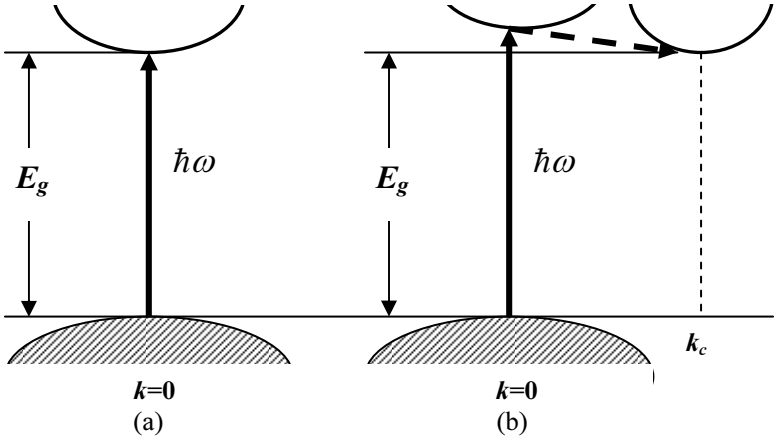

Figure 2.3 Optical absorption process for (a) a direct band gap (b) an indirect band gap

Figure 2.3 shows the schematic diagram of the interband transitions of direct and indirect bandgap semiconductors. As briefly mentioned in the previous section, typical optical band to band transitions of a direct band gap semiconductor is allowed by electric dipole transition [5]. Since, the direct bandgap absorption and corresponding emission processes is vertical as depicted in figure 2.3 (a), the life-time of emission is expected to be fast. Significantly rapid

radiation within the nanosecond range will lead to very efficient luminescence which is often achieved by typical direct bandgap semiconductors. The absorption coefficient for a semiconductor with parabolic band is described by

$$\text{For } \hbar\omega < E_g, \ \alpha(\hbar\omega) = 0$$

$$\text{For } \hbar\omega \geq E_g, \ \alpha(\hbar\omega) \propto (\hbar\omega - E_g)^{\frac{1}{2}} \tag{2.3}$$

where $\hbar\omega$ is the energy of photons and E_g is the bandgap of the material. Obviously, there is no absorption if the applied photon energy is less than the bandgap energy. Absorption increases as $(\hbar\omega - E_g)^{\frac{1}{2}}$ for photon energies greater or equal to the bandgap and such materials are expected to have their threshold at exactly E_g.

The general aspect of an indirect band gap transition is rather complicated. As shown in figure 2.3 (b), there is also emission of a phonon to conserve the momentum of the transition process. Therefore, it is not possible for a electron to be promoted from the valence band to the conduction band without a change in momentum. By deriving the quantum mechanical transition rate for an indirect gap semiconductor, it gives the following result:

$$\alpha^{indirect}(\hbar\omega) \propto (\hbar\omega - E_g \mp \hbar\Omega)^2 \tag{2.4}$$

This explains the absorption have a threshold not exactly at E_g. The difference is $\mp\hbar\Omega$ (required wave vector) depending on whether the phonon is absorbed or emitted. In a similar manner to absorption, emission from an indirect gap material requires a phonon process. The probability of such a process is much smaller than the direct gap process, making indirect gap semiconductors such as silicon very inefficient light emitters.

2.2.2 Urbach Edge (Tail)

There are some direct gap materials that exhibit an optical absorption edge different from equation 2.3 under certain circumstances. They show the so-called Urbach edge or tail

which is often observed in doped semiconductors. The Urbach tail is an exponential distribution of absorption states at energy less than E_g, and is most often attributed to defects breaking down the long range symmetry of the crystal [5]. By implying an empirical form for the absorption coefficient, the Urbach edge can be described by

$$\alpha = \alpha_0 \exp\left[\gamma\left(\hbar\omega - E_0\right)/ k_B T\right] \tag{2.5}$$

where γ is a constant, E_0 is an effective gap, and T is temperature. This type of behaviour has a more gradual dependence on photon energy than absorption from a pure direct gap material and the edge becomes broader as temperature increases [4].

2.2.3 Burstein Moss effect

The energy of the measured optical absorption edge depends strongly on the electron concentration. The significant blue shift of the absorption edge or photoluminescence can be fully accounted for by the Burstein-Moss shift [5]. It is an interesting example of the consequences of direct transitions and understanding its process is a vital aspect for the optical measurements. Also, it may explain the relatively high band energy gap of 1.9 eV from previous report may be attributed to prominent band filling effect at the conduction band.

In semiconductors with a very high electron concentration, ~10^{19}-10^{20} cm^{-3}, the number of empty states near the bottom of the conduction band is much reduced. Optical absorption of electrons from the valence band then has to bypass energies near the conduction band minimum and promote electrons into higher states. The effect is to “blueshift” the absorption edge. Since the electron concentration can be changed with doping or unintentional impurities or defects, a simple absorption measurement may not reveal the true bandgap energy E_g.

In a corresponding manner to absorption, the Burstein-moss effect can also cause a “blueshift” in the observed photoluminescence spectra. The measured spectrum consists of transitions of electrons recombining with holes, from all occupied conduction band states. At low concentration of n, only states near the band minimum are occupied and PL is a close

representation of E_g. However, the transitions with a high concentration of electrons occur from the upper conduction band states which give higher energy emission.

In PL the Burstein-Moss effect can be enhanced by the optical excitation that is sometimes used. As the excitation intensity increases, transitions from higher states become stronger leading to a slight shift of the peak energy to the blue.

2.3 Photoluminescence

2.3.1 Introduction

The general term "Luminescence" describes light emission from a body that is not due to blackbody radiation. In semiconductors luminescence occurs when excited electrons recombine with holes or traps and a photon is emitted. However, there are many mechanisms of exciting the electrons and each type gives a different name to the luminescence. The more common kinds for studying semiconductors are given in table 2.1 and associated with the excitation source.

Table 2.1 The commonly used luminescence types and their excitation sources.

Luminescence type	Excitation sources
Photoluminescence (PL)	Photon excitation
Electroluminescence (EL)	Injection of electrons and holes via external current
Cathodoluminescence (CL)	Electron gun excitation

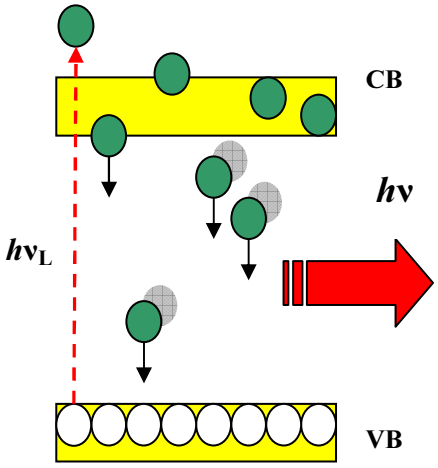

Figure 2.4 Schematic diagram of photoluminescence process during the recombination of electrons and holes. The photon is emitted when the electrons relax down to the valence band via the band energy gap.

The photoluminescence (PL) is perhaps the most common technique as it requires a simple excitation source, usually a laser, and is non-contact meaning that samples do not require post-growth processing. As mentioned above, light emission arises from the relaxation of an electron to a lower state (see figure 2.4). However, there are many possible starting and finishing levels for the electrons and the following section discusses some of these.

2.3.2 Emission Spectroscopies

There are several numbers of potential transitions which lead to luminescence governed by the localization of each state as shown in figure 2.5.

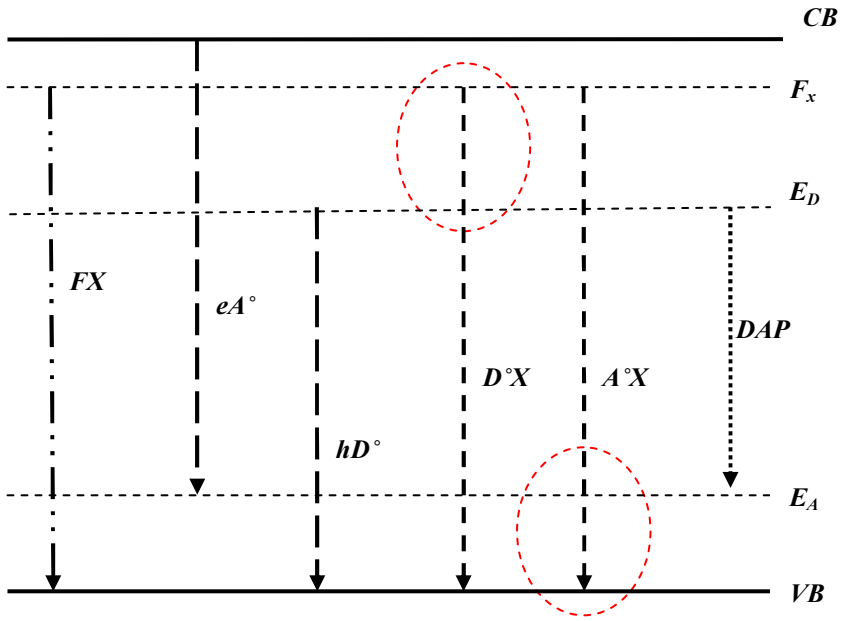

Figure 2.5 The schematic diagram of possible transitions during Photoluminescence. (*CB*=Conduction band, F_x=Free exciton state, E_D=Donor level, E_A=Acceptor level, *VB*=Valence band.)

Exciton – The excited state is created when the electrons are excited from the valence band (create holes) to the conduction band by the energy of the incoming radiation being greater than or equal to the bandgap. Subsequently electrons and holes move freely within the respective bands according to dynamics requirement such as mobility, relaxation time and effective mass. When the electron and hole are uncorrelated with each other the excited state has an energy of the bandgap E_g. However, there is also a lower energy excited configuration below E_g which is known as exciton, Here the electron and hole are correlated. Generally, there are two main types of excitons, free (large radius) and Frenkel (small radius) excitons. They can be formed by photon absorption any place in the Brillouin zone $\partial E_v / \partial k = \partial E_c / \partial k$ at the same *k*-value. Therefore, the group velocities of the electron and hole are equal and the particles may be bound closely together. The bound exciton state has "hydrogenic-like" energy levels with the ground state below the bandgap energy E_g. The difference between the exciton ground state and E_g is the exciton binding energy and is the energy required to completely separate the electron and hole. For GaN the exciton binding energy is around 28 meV which means that elevated sample temperatures can destroy the exciton.

However, at low temperatures PL from excitons can be observed at energies just below E_g as shown in figure 2.5. It is in such spectral regions that there is little background absorption to interfere with the observation. Depending on exciton type, its characteristic may be different but in general, excitons can be recognized by the temperature dependent PL. Since the electrons and holes are tightly bound due to the same *k*-value, its radiation life time is expected to be relatively short.

Free to bound transitions – Doped semiconductors have impurity energy levels positioned in the bandgap; donor levels just below the conduction band and acceptors just above the valence band. Donors and acceptors are thermally ionized from their neutral state to provide carriers in their respective bands. However, at low temperatures many of the donors and acceptors remain neutral and can participate in an emission process (hD$^\circ$ and eA$^\circ$). For example a free electron in the conduction band can relax to the neutral state of the acceptor as shown in figure 2.5. The corresponding donor transition is an electron from a donor level relaxing to a hole state in the valence band. The energies of these transitions are

$$E(\hbar\omega) = E_g - E_A(E_D) \tag{2.6}$$

where E_A, E_D are the acceptor and donor level energies respectively. Since these transitions involve a free carrier they are designated free-to-bound transitions.

Bound Exciton – The excitons described in the previous section can be labelled “free” because this system is able to move through the lattice for a short time before recombination of the electron and hole. However, before recombination takes place there is a chance that the exciton becomes “bound” to a defect – common defects are native or doped donors or acceptors. The recombination emission from such a bound exciton is less than free exciton emission *FX* by the donor or acceptor energy ie

$$\begin{aligned} E(D^\circ X) &= FX - E_D \\ E(A^\circ X) &= FX - E_A \end{aligned} \tag{2.7}$$

Here $D^{\circ}X$ and $A^{\circ}X$ are labels used for donor and acceptor bound excitons. A small amount of thermal energy can induce the exciton to break free of the dopant and thus bound exciton emission intensity decreases faster as the temperature is increased.

Donor-acceptor pair (DAP) - The donor-acceptor pair (DAP) transition is often observed from p-type semiconductors and is attributed to the electrons from the donor level recombining with holes on the acceptors. The electron and hole orbits overlap slightly when a neutral donor and acceptor are close enough that electron and hole can recombine and emit light. The energy of a DAP transition is

$$\hbar\omega = E_g - E_A - E_D + e^2/(\varepsilon R)\,. \qquad (2.8)$$

The origin of the last term $(e^2/(\varepsilon R)$ is attributed to the Coulomb attraction of the pair of donor and acceptor. The direct evidence of DAP transition in luminescence is the indication of blue shifts as a function of excitation intensity.

2.3.3 Temperature Dependent Features

The temperature dependence is one of the vital parameters in understanding luminescence mechanisms. Generally, most semiconductors have a pronounced red shift for emission energy as temperature rises due to significant bandgap shrinkage. This phenomenon can be illustrated as the relaxation of the crystal lattice spacing which at low temperatures contracts increasing the potential between neighbouring atoms. The electron-lattice interaction can also change the bandgap with temperature. Phenomenologically, the interband emission peak energy follows the well known Varshni formula

$$E_g(T) = E_g(0) - \alpha \cdot T^2/(T+\beta) \qquad (2.9)$$

where $E_g(T)$ is the band gap at an absolute temperature T. The coefficients α and β are the

electron-phonon interaction with thermal expansion and the physics associated with the Debye temperature of the crystal [8].

The Arrhenius fit also takes very important role in a detailed analysis of PL temperature dependence. The variation of integrated PL intensity as a function of temperature can divulge the thermal activation energies of the each transition as given by the equation

$$I(T) = \frac{I(0)}{1 + C\exp\left(-\frac{E_a}{kT}\right)}, \tag{2.10}$$

where E_a indicates the activation energy and k is the Boltzmann constant. Parameters in a fit of I versus T can be $I(0)$, C and E_a although in most cases $I(0)$ can be taken as the measured intensity at a helium cryogenic temperature.

However, considering the wide range of temperature variation during the PL measurement, the single activation energy E_a plot may not be sufficient and it often shows the limitation for plot fitting. Thus, a modification of equation 2.10 has been made to improve the fitting and for further interpretation of optical properties. The thermal activation energies can be determined by the equation,

$$I(T) = \frac{I(0)}{1 + C_1\exp\left(-\frac{E_{a1}}{kT}\right) + C_2\exp\left(-\frac{E_{a2}}{kT}\right)}, \tag{2.11}$$

where E_{a1} and E_{a2} are the thermal activation energies at low and high temperature, respectively and the coefficients C_1 and C_2 describe the strengths of quenching processes. The efficiency of luminescence and the origin of the localized energy can be comprehensively determined by an Arrhenius plot with two thermal activation energies.

2.4 Experimental Consideration

2.4.1 Introduction

The basic elements of optical spectroscopy experiments complement the general aspects of the light. M. Sobin *et al*. described that there are three stages in the life of a light beam: it is created, it travels through space, and it is destroyed. The light is created and destroyed only via its interaction with matter, from glowing gases in the sun to rhodopsin in the eye [9].

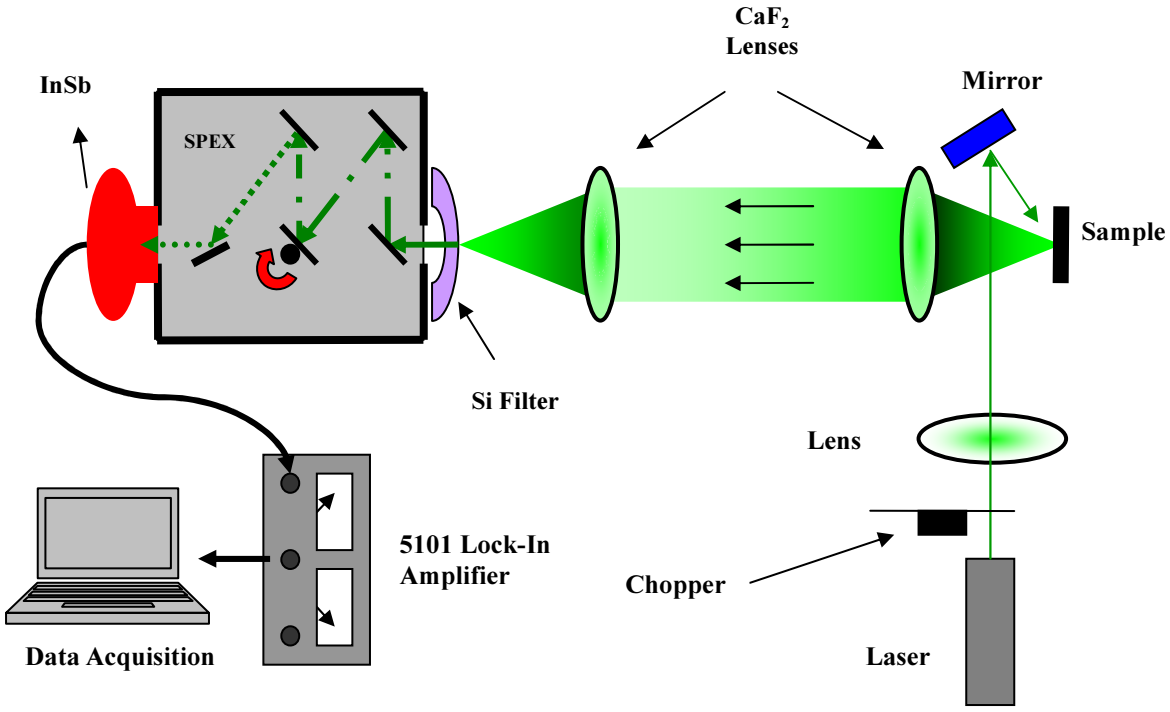

Figure 2.6 A schematic diagram of the experimental setup used for photoluminescence

The laser spectroscopy requires three major components; a light source, a dispersing element and a detector. Figure 2.6 show a schematic diagram of the experimental setup used for photoluminescence (PL). For this study of the luminescence from doped InN a variety of devices are employed such as Argon and diode lasers, InSb detector, Minimate spectrometer,

CaF_2 lens etc. In this section, the consequence of each component is discussed and their roles will be illustrated.

2.4.2 Components

Laser - Two excitation lasers were used to obtain PL spectra in this research. The Mg and Ca doped InN was excited with a DPSS-60 diode laser with a wavelength of 532nm and an output power of 60mW. For Zn doped samples, the 488nm line of a Spectra-Physics model 2080 argon laser was used with an output power of 100mW~1W. Due to a low PL signal from Zn doped InN, a higher excitation power was necessary. To accurately measure the excitation power, a laser power meter was placed in the beam path just before it strikes the sample inside the cryostat. To maximize the PL from the sample, the laser beam was focused by a lens to give an excitation intensity of irradiating area of 3.8 W/cm^2 for both the diode and argon lasers.

Lens - Two CaF_2 lenses with focal lengths of 100 and 200 mm were employed to collimate the PL and refocus it into the entrance slit of the spectrometer. Earlier workers had determined that unwanted absorption dips were occurring in measured spectra. These dips were traced to OH vibration within the quartz lenses used at that time. By introducing CaF_2 lenses, these dips were reduced although not totally minimized due to atmospheric water absorption. The *f* numbers of both lenses were chosen carefully to prevent any loss of light. Finally, in order to achieve the maximum PL signal the positions of the two lenses were optimized vertically and horizontally.

Cryogenics – In order to maintain a low temperature during the experiment, the sample is placed in an Oxford He Microstat. The cryostat is connected to a helium storage dewar with a transfer tube which allows the helium gas to flow continuously during the experiment. The lowest temperature inside the cryostat which can be achieved is 3.5 K as the pressure is less than 1 atmosphere. The doped InN films were mounted on the sample holder using high

thermal conductivity silver paste. The sample holder is designed to be attached to the tip of the heat exchanger where a heater and temperature sensor are located. The temperature sensor is a silicon diode mounted on the back of the baseplate and resitive heater is used for variable temperature operation. The temperature inside the cryostat is monitored and automatically controlled by an Oxford temperature controller allowing precise temperature dependent PL measurement to be made.

Minimate SPEX – The PL emission was dispersed and analyzed by a "0.25M Spex Minimate". In order to maximize the signal, the entrance slit of the spectrometer was fully opened at 320 μm. The 300 line grating blazed at 2.4 μm was employed inside the spectrometer. Rotation of the grating is controlled by a stepper controller for PL measurement over the desired wavelength range. The spectrometer has been calibrated as 105 steps from the motor equal 1.0nm step of the PL spectra. A silicon filter was required at the entrance slit of the spectrometer to suppress detection of any scattered laser signal. InN emits a relatively small PL signal so chromatic aberration is a considerable concern. In optics, chromatic aberration is a distortion caused by a lens due to the wavelength dependent refractive index. For instance, the term "purple fringing" is commonly used in photography and it is caused by chromatic aberration. Altering the placement of the lens can noticeably change the shape of the PL signal. Mg doped sample with strong PL emission was used to examine chromatic aberration by adjusting the longitudinal position of the lenses.

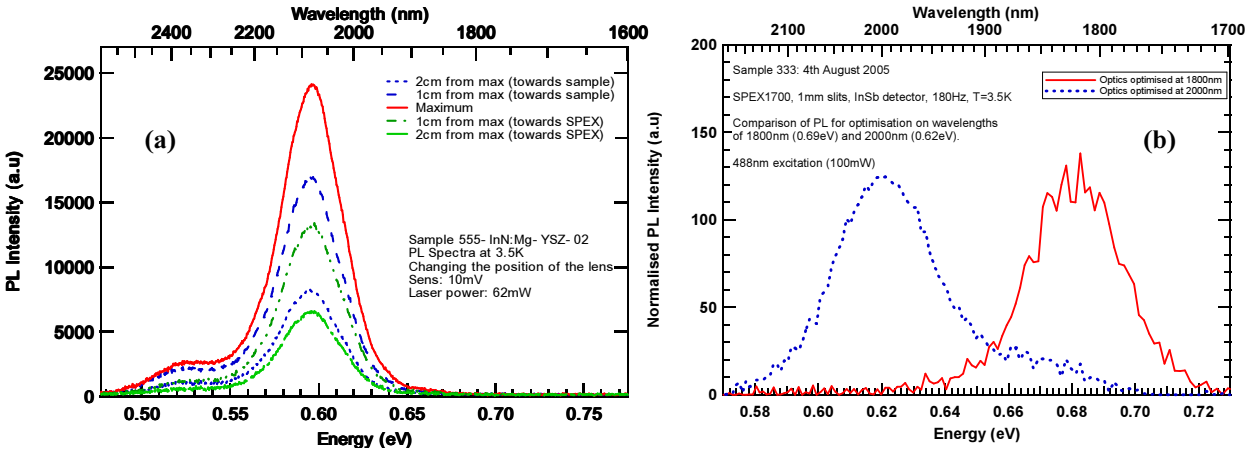

Figure 2.7 (a) The PL response of sample 555-InN:Mg with different lens positions using the Minimate. (b) The effect of chromatic aberration with a 1m spectrometer (SPEX 1700).

Figure 2.7 depicts the effect of chromatic aberration using two different spectrometers Minimate and SPEX 1700. Fortunately, no prominent effect of chromatic aberration was observed for the Minimate. It might be attributed to the significantly smaller size of Minimate.

Detector – A Judson J10D series liquid-nitrogen-cooled InSb detector was used to detect the PL signal. The employment of InSb detector is strongly recommended since its wavelength range of 1~3.3μm is the most suitable for InN. The detector is coupled with a PA-9 preamplifier from Judson that was used in its 2nd stage AC mode. The PL signal from the InSb detector is conveyed to the Lock-in via the preamplifier.

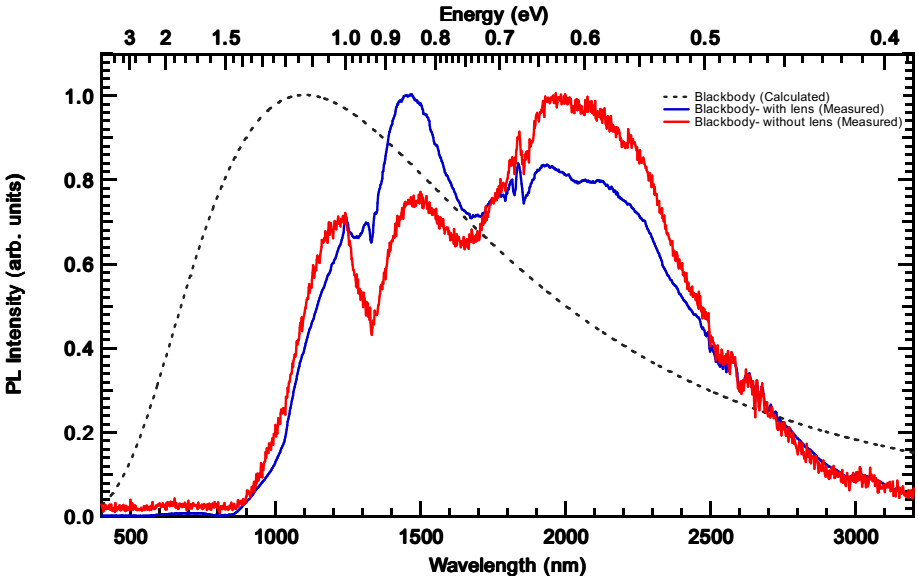

Figure 2.8 Comparison between the calculated blackbody radiation curve (black dotted line) and the blackbody radiation detected with the InSb detector. A Tugsten coiled quartz iodine lamp (2500 K) was used for the light source at room temperature

Figure 2.8 demonstrates the comparison between the calculated and detected blackbody radiation using the InSb detector. A Tungsten coiled quartz iodine lamp was the blackbody source. The consequence of this experiment was to verify the background PL response from the detector by submitting the scaled value from the compared blackbody radiation into the raw data. The several dips in the measured spectra are due to grating notches and OH absorptions.

2.4.3 Data Acquisition

The signal from the sample was optically optimized at the entrance slit of the spectrometer. The Minimate spectrometer is commanded by a stepper drive via a home built controller which scans the desired wavelength range. The scanning range for InN was chosen to be from 1600nm to 2400nm. The exciting laser beam was mechanically chopped with a rotating blade chopper. A DC signal from the lock-in was digitized and recorded by the PC computer controlling the spectrometer scan.

The time constant on the lock-in was kept deliberately short, ~100ms, so that a fast response was obtained. Signal averaging was done by integrating the digitized output voltage. The computer data recorded was graphed and analyzed in the commercial program Igor Pro.

2.5 References

[1] F. Bechstedt. J. Furthmuller. M. Ferhat. L. K. Teles. L. M. R. Scolfaro. J. R. Leite. V. Yu. Davydov. O. Ambacher and R. Goldhahn. Phys. Stat. Sol. (a), **195** (2003) 628

[2] P. A. Anderson 2006 *Indium Nitride: An Investigtion of growth, electronic structure and doping* Ph.D Thesis (University of Canterbury)

[3] M. Fox, Optical Properties of Solids. Oxford, New York, 2001

[4] G. Burns, *Solid State Physics Academic Press*, INC. New York 1990

[5] K.Krane, *Mordern Physics* John Wiley and Sons, Inc, Canada, 1996

[6] A. A. Klochikhin, V. Yu. Davydov, V. V. Emtsev, A. V. Sakharov, and V. A. Kapitonov, Physical Review B **71**, 195207 (2005)

[7] W.Walukiewicz, S. X. Li, J. Wu, K. M. Yu, J. W. Ager III, E. E. Haller, H. Lu, andW. J. Schaff. Journal of Crystal Growth 269 (2004) 119-127

[8] C. Hsiao, H. Hsu, L. Chen, C. Wu, C. Chen, M. Chen, L. Tu and K, Chen, Appl. Phys. Lett. **91**, 181912 (2007)

[9] M. Sobin *Light*, p. 73, University of Chicago Press,1987.

Chapter 3 Mg-doped InN

3.1 Overview of the Results

To investigate the optical properties of p-type InN, twelve films of Mg:InN were prepared in this research. All Mg doped InN samples used in this study were produced locally at the University of Canterbury. The films were grown on YSZ substrates by molecular beam epitaxy (MBE) with various Mg cell (T_{Mg}) temperatures to provide varying Mg concentrations. The substrate temperature for the InN layers was at 450 ˚C and In cell temperature maintained at 780 ˚C for N-rich growth conditions. The following section presents the optical results from the individual samples while this first section provides a brief overview.

Table 3.1: Mg-doped InN Samples produced by Electrical and Computer Engineering Department.

Sample Number	T_{Mg} (˚C)	Mg concentration (cm^{-3})	Peak position (eV)	Peak Intensity (a.u)	Carrier Concentration (cm^{-3})	Hall Mobility (cm^{-2}/Vs)
579-InN:Mg	170	5.2×10^{17}	0.68	8200	2.03×10^{19}	164
577-InN:Mg	200	1.3×10^{17}	0.68	9900	1.84×10^{19}	196
601-InN:Mg	208	2.7×10^{17}	0.67	1800	1.53×10^{19}	196
585-InN:Mg	216	6.2×10^{17}	0.60	3500	4.71×10^{18}	295
590-InN:Mg	220	3.7×10^{17}	0.68	250	2.00×10^{19}	60
555-InN:Mg	225	8.7×10^{17}	0.60	12300	7.31×10^{18}	16
594-InN:Mg	230	1.5×10^{18}	0.61	800	1.46×10^{19}	190
580-InN:Mg	240	3.3×10^{18}	No PL	No PL	1.60×10^{19}	110
584-InN:Mg	260	1.2×10^{19}	No PL	No PL	1.72×10^{19}	100
583-InN:Mg	276	3.6×10^{19}	No PL	No PL	6.82×10^{18}	16
557-InN:Mg	300	1.0×10^{20}	No PL	No PL	1.86×10^{19}	5
554-InN:Mg	370	-	No PL	No PL	-	-

Note: Peak intensities are normalized to 10mV lock-in sensitivity

Table 3.1 summarizes the general details of electrical and optical properties of a series of Mg doped InN films. It presents the Mg cell temperatures during the growth and peak positions and relative intensities for PL measurements. The electrical data was recorded by students from the growth group in the Electrical and Computer Engineering Department. Most of the samples with PL responses revealed an n-type behaviour by capacitance-voltage (CV) due to the electron accumulation layers on the surface of InN film. This proves the difficulties in creating the demonstration of p-type InN. Also it may be attributed to the low activated Mg acceptor concentrations being not enough to exceed residual donor concentration [1]. To evaluate the Mg dopability of InN, a series of InN:Mg samples have been analyzed by SIMS (secondary ion mass spectroscopy). The Mg cell temperatures (T_{Mg}) range from 170 to 370 ˚C during growth has been converted to Mg concentration, which is normally in proportion. The semilogarithmic plot of the Mg concentration as a function of the sputtering time is displayed in figure 3.1 and estimated Mg concentrations in each InN film are also shown in table 3.1.

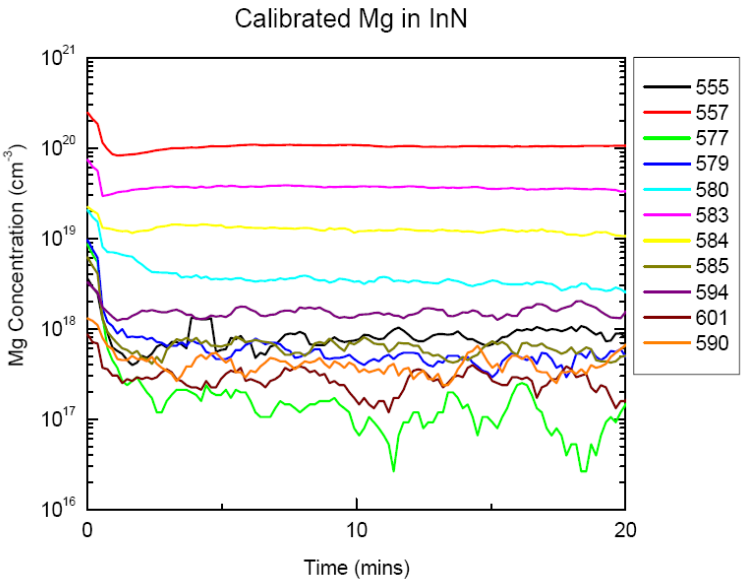

Figure 3.1 The SIMS measurement for the series of Mg doped InN. The list of T_{Mg} converted into Mg concentration (cm^{-3}) for each sample. The Mg concentration is proportional to Mg cell temperature. The time (min) is representing the sputtering time. (Data from Warwick University).

The optical properties of Mg doped InN is characterized by photoluminescence (PL) measurements using a 532nm diode laser and an InSb detector. The temperature and power dependence of the PL emission revealed some fundamental optical properties of Mg doped InN. The success in achieving PL emission from Mg doped InN as shown in figure 3.2 (a), provides strong evidence that Mg is a suitable p-type dopant for InN.

The PL spectra of Mg doped InN series yielded two different characteristics. They have been divided into two groups in accordance to the Mg concentration and T_{Mg} in the samples and

categorized by the energy of peak emission. Figure 3.3 summarizes the observed PL spectral peak positions of each sample as functions of T_{Mg} variation and Mg concentrations. It has been demonstrated in figure 3.3 that samples with low T_{Mg} (< 210˚C) have their peak emission at 0.68 eV. Meanwhile, the samples with high T_{Mg} (> 210˚C) have their peak emission centered near 0.6 eV.

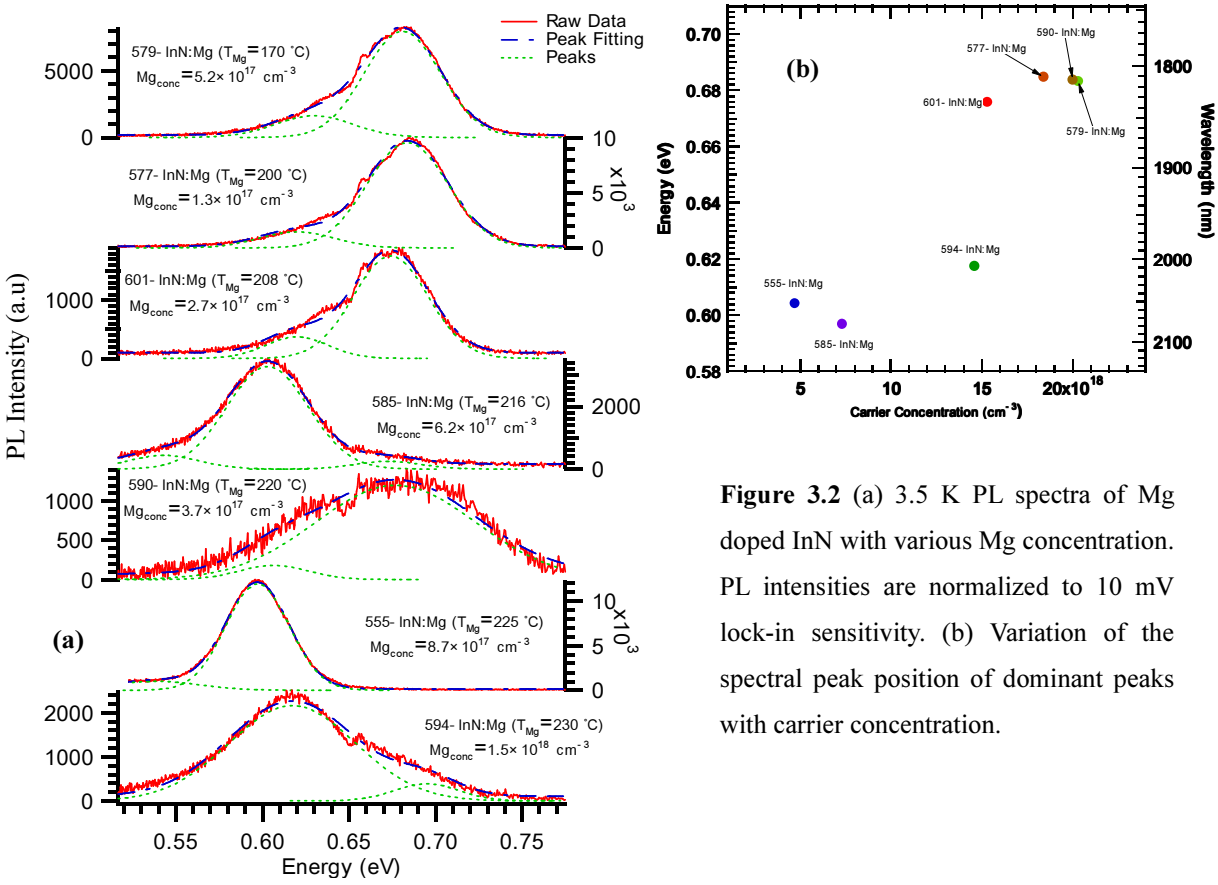

Figure 3.2 (a) 3.5 K PL spectra of Mg doped InN with various Mg concentration. PL intensities are normalized to 10 mV lock-in sensitivity. (b) Variation of the spectral peak position of dominant peaks with carrier concentration.

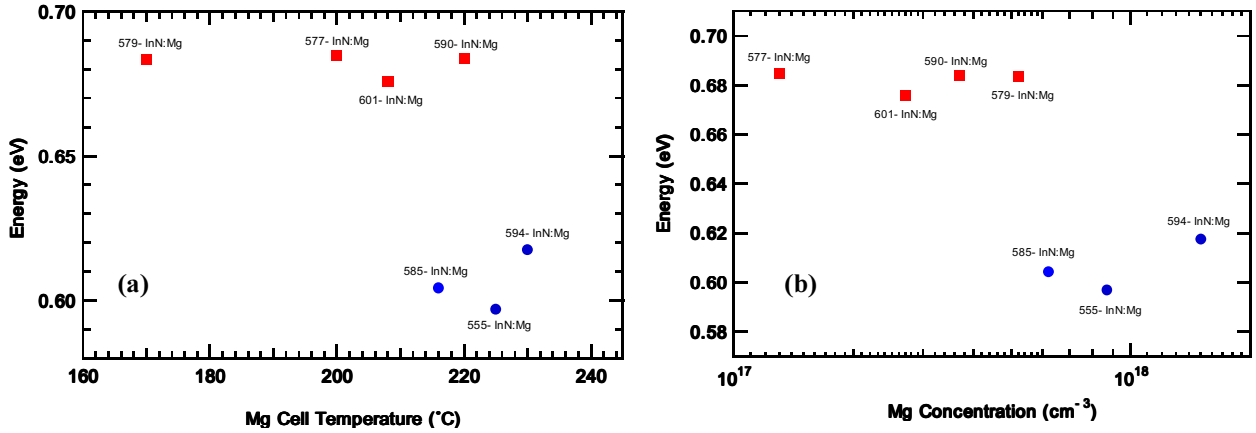

Figure 3.3 Variation of the dominant peaks with (a) different Mg cell temperature and (b) different Mg concentration (log).

The sample 555-InN:Mg with T_{Mg}=225 ˚C was the first film to produce detectable PL and provide potential evidence that InN with significant amount of doping is capable of light emission. There was no indication of PL in previous attempts on the sample 554 and 557-InN:Mg which may be influenced by their relatively high T_{Mg} of 370 and 300 ˚C, respectively. The samples with relatively high T_{Mg} (210~230 ˚C) such as 594, 585 and 555-InN:Mg pronounced noticeable shift of 0.1 eV from unintentionally doped InN (~0.7 eV).

The other circumstance worth noting is no indication of a dramatic peak shift of the dominant transition for samples with low T_{Mg}. The sample 579-InN:Mg was grown with relatively low T_{Mg}=170 ˚C and PL measurement was performed after achieving prominent results from 555-InN:Mg. Although the dominant transition was centered at 0.68 eV, a peak near 0.6 eV was clearly maintained. Subsequently, T_{Mg} was raised up to 200 ˚C (sample 577) to regulate the optical properties of InN with Mg concentration variation. The PL response from sample 577 as displayed in figure 3.2 (a) resembled sample 579 in that its dominant peak remain centered at 0.68 eV. This behaviour is similar to that seen in previous reports for unintentionally doped InN [4,7,13]. Despite the fairly high Mg concentration in sample 590-InN:Mg, its emission peak is located at a relatively high energy of 0.68 eV. However, the PL intensity from 590 is anomalously weaker and it has a carrier concentration significantly higher than its immediate neighbours as shown in figure 3.2 (b).

From the spectral fitting the intensity of the peak near 0.68 eV was extracted for each sample. The intensity of this peak as a function of T_{Mg} and Mg concentration are graphed in figure 3.4. It is clearly shown in the figures that the peak intensities are drastically affected by T_{Mg} and Mg_{conc}. PL intensity dropped by more than two orders of magnitude as T_{Mg} went from ~150~240 ˚C. This result is consistent with the previous report on Mg doped InN by Wang *et al* [1]. Further, no detectable PL was observed for high concentrated Mg films with T_{Mg} above 240 ˚C (Mg_{conc}= 3.3×10^{18} cm^{-3}). This may be attributed to unknown luminescence killer processes such as sheet charge accumulation at the surface of the film or Auger processes. Thus, the origin of the PL quenching in heavily doped p-type InN still requires more interpretation. However, the observed PL spectrum from samples with low Mg concentrations indicates a significant step toward a feasible InN pn junction.

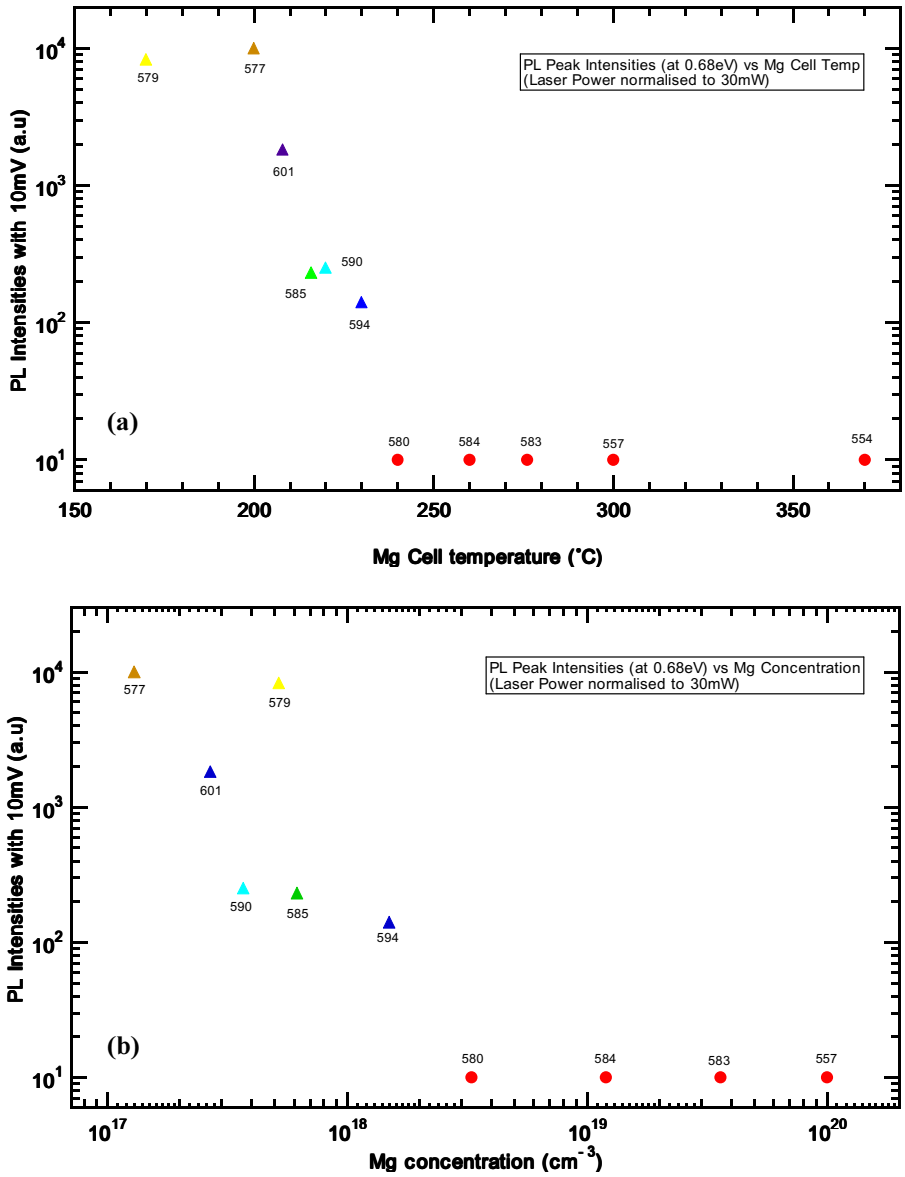

Figure 3.4 Normalized (10mV) PL intensities at energy 0.68 eV of InN:Mg at 3.5K (a) as a function of Mg cell temperature and (b) as a function of Mg concentration. (No indication of peak at 0.68 eV for the sample 555-InN:Mg). The sample designation of red dots indicates no detectable PL.

Fundamentally, it is difficult to determine the origin of dominant peaks of each film with a single plot. Also conflicting discussions about the fundamental properties of InN are often found in the literature. However, considering the several similarities between InN and GaN, the origin of dominant peaks can be estimated as luminescence from deep or shallow acceptors in InN. For further investigation on Mg doped InN, the detailed analysis of each transition will be discussed in the next section with excitation intensity and temperature variation.

3.2 Characterization

There are still formidable questions regarding the optical properties of Mg doped InN. For instance, there are conflicting arguments [1,2,5,12] about the origin of certain transitions and the PL quenching in heavily doped InN remains unexplained. Thus the detailed PL spectra with excitation power and temperature changes have been comprehensively investigated and discussed. The shape and energy position of emission spectra has been analyzed simultaneously and taking into account specific peculiarities at high and low Mg concentration, fundamental properties of doped InN has been studied. An additional evaluation supporting the results is given by plotting Arrenhius and Varshni's fit to yield thermal activation energy and bandgap, respectively for each film.

3.2.1 Sample 579: $Mg_{conc} = 5.2\times10^{17}$ cm^{-3}

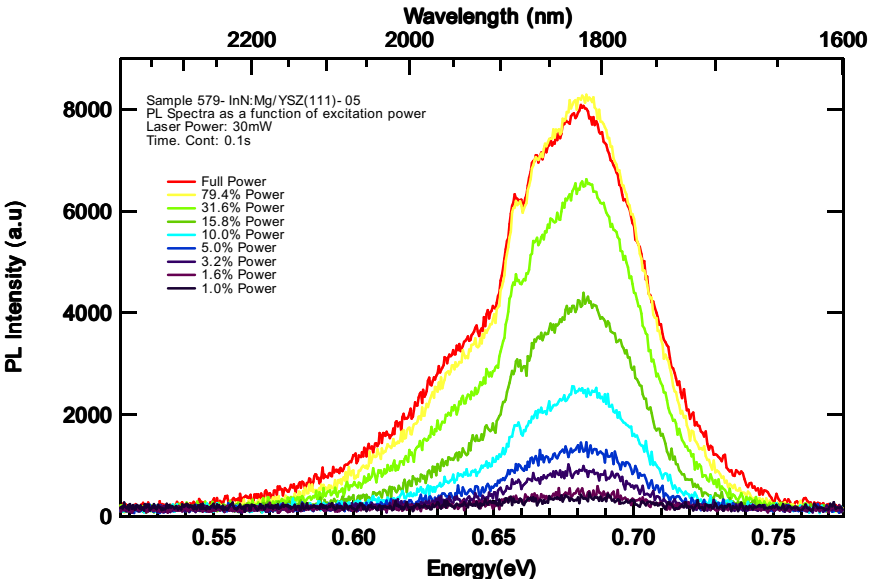

Figure 3.5 Power dependent PL measured at 3.5K with InSb detector was used. PL measured at Lock-In sensitivity 10mV with 1 second integration time. T_{Mg} = 170 ˚C (Mg_{conc}=5.2×10^{17})

The sample 579-InN:Mg was grown with the lowest Mg cell temperature of (T_{Mg}) ~170 ˚C. Figure 3.5 shows detailed PL spectra recorded at 4 K as a function of excitation power. The excitation power was controlled by calibrated optical density (OD) filters. The PL spectra consist of a main peak at an energy of 0.68 eV and a lower energy shoulder near 0.63

eV that is more apparent at high excitation powers. Unfortunately, the spectra are slightly perturbed by a grating imperfection at 0.65 eV. The data analysis software package IGOR was used to peak fit individual lines to the spectra and the results of this fitting are presented in figure 3.6. The data fitting process returned PL line parameters such as position and intensity.

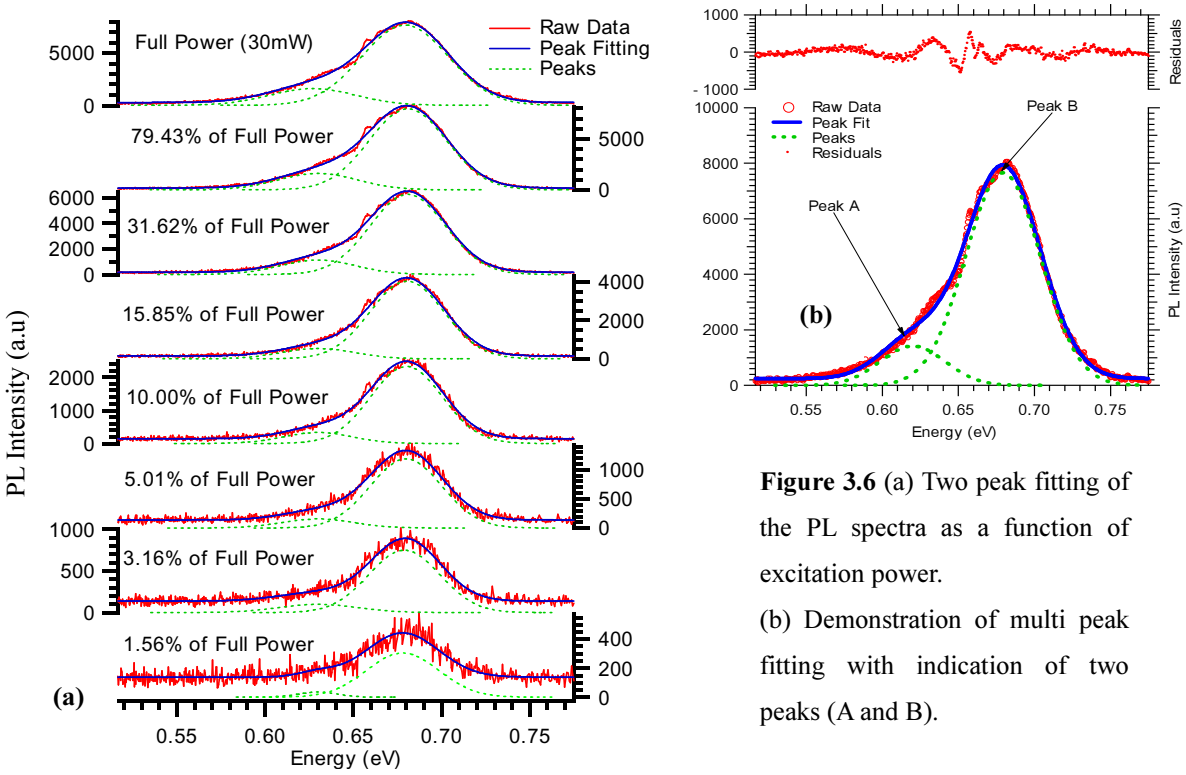

Figure 3.6 (a) Two peak fitting of the PL spectra as a function of excitation power.
(b) Demonstration of multi peak fitting with indication of two peaks (A and B).

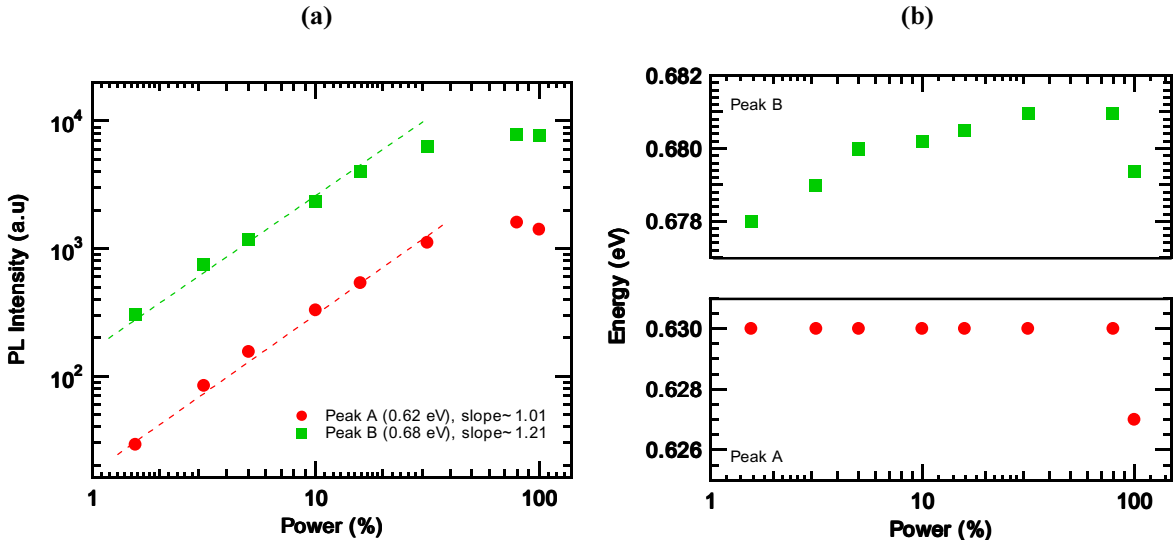

Figure 3.7 (a) Integrated intensity vs power with straight line fit. (b) Peak positions for peak A and B as a function of power.

Figure 3.7 (a) shows the integrated intensity as a function of excitation power. The PL intensity of both spectral peaks shows the similar linear dependence on the log scale indicating linear excitation processes. Both straight line fits yield slopes close to 1 which is consistent with the transitions in direct bandgap semiconductors. Above 30% of maximum power there is a very clear saturation of the intensity.

The simultaneous peak energy fit in figure 3.7 (b) explains that there is no peak shifting correlation between two peaks. The main peak (peak B) at 0.68 eV exhibits a blueshift with increasing power up to 30% of maximum. This shift is attributed to the band filling Burstein-Moss effect [1] as discussed previously [See chapter 2]. The amount of blue shifting is more apparent at low excitation power region because the density of states decreases as the transition is made closer to the bottom of conduction band. Meanwhile, peak A (0.62eV) yields significantly stabilized behaviour with power variation. It is worth noting that, above 30% power, the peak position begins to shift back to the red. This observation combined with the saturation of intensity at the same power suggests that significant sample heating is occurring at these higher powers.

The dominant peak (peak B) centered at energy of 0.68 eV has two possible origins. It could be considered as recombination of free electrons with holes in acceptors by taking account of the equation $hv = E_g - E_a + kT/2$ (binding energy) [2,4]. It could also be the donor and acceptor pair (DAP) transition due to relatively low peak energy compared to unintentionally doped InN (~0.7 eV). If the emission is from DAP transition the prominent blue shifting is caused by the coulomb interaction between electrons and hole which is associated with the equation $hv = E_g - E_A - E_D + (e^2/\varepsilon R)$. It is worth noting that despite this sample being grown at the lowest T_{Mg}, the measured Mg concentration of this film by SIMS was significantly high ($Mg_{conc} = 5.2\times10^{17}$ cm^{-3}). Thus, by considering the relatively high Mg concentration of this film, the PL emission of peak B (0.68 eV) is most likely to be attributable to the electron transitions to the shallow acceptor states (Assumption that no occurrence of native defects act as acceptors).

In similar fashion, the origin of peak A (0.62 eV) can be ascribed as the free electron to deep or shallow acceptor level (free to bound). It is not likely to be DAP transition since there was no evidence of any shifts as a function of excitation power. Also by estimating the binding energy at the peak 0.62 eV, it fully agrees with the results in Ref. 6 indicating the peak near 0.62 eV as the transition from deep acceptors.

3.2.2 Sample 577: $Mg_{conc} = 1.3\times10^{17}$ cm^{-3}

The sample 577 was grown in a relatively similar condition with the sample 579. The T_{Mg} of this film during growth was 200 ˚C. Figure 3.8 (a) shows PL spectra recorded as a function of excitation power. Consistent with previous observation of the sample 579, the PL spectra for sample 577 indicates of a main peak at an energy of 0.68 eV and a lower energy shoulder near 0.63 eV that is more apparent at high excitation powers. For further interpretation in the optical properties of sample 577, PL has been measured at different temperatures at full excitation power ~30mW as displayed in figure 3.8 (b). Qualitatively, the changes in the spectra with increasing temperature are similar to those occurring with decreasing excitation power. The correlation between the power and temperature dependence allow characterization of prominent features.

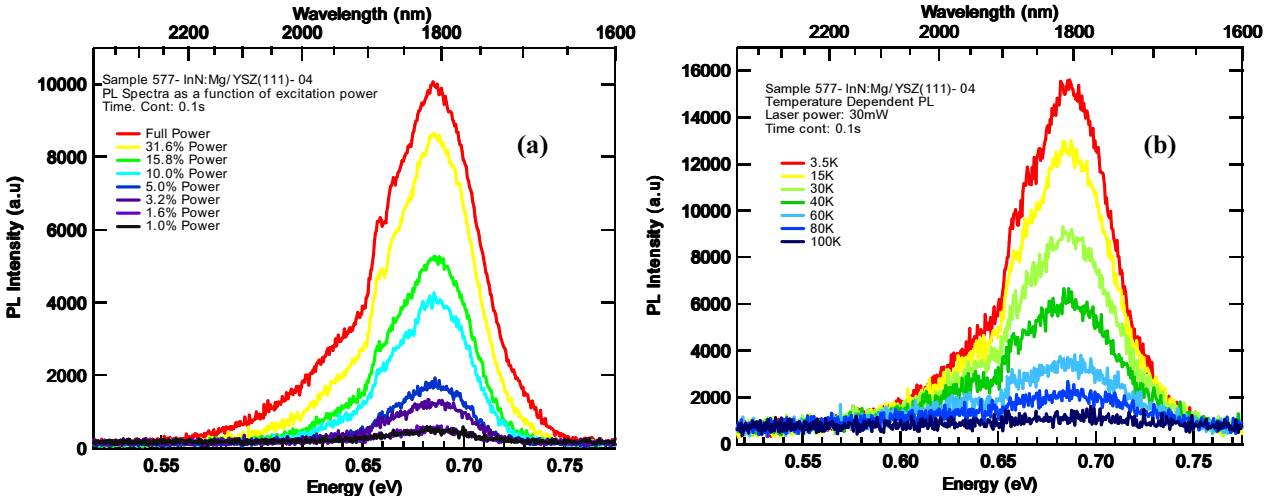

Figure 3.8 (a) PL Spectra as a function of excitation power for sample 577-InN:Mg. PL measured at 3.5K with 532nm laser excitation and InSb detectors. Lock-In sensitivity was 10mV with 1s integration time. **(b)** Temperature dependent PL for sample 577-InN:Mg with constant full excitation power (30mW). 2.5mV Lock-In sensitivity with 1s integration time.

Both data have been analyzed by individual peak fitting and the plots are presented in figure 3.9. Their dominant PL emission peaks at 0.68 eV gradually decreased as a function of excitation power and temperature. It is worth noting that, peak A (0.63 eV) disappeared below 3.18% of maximum laser power and the same process was observed above 100 K.

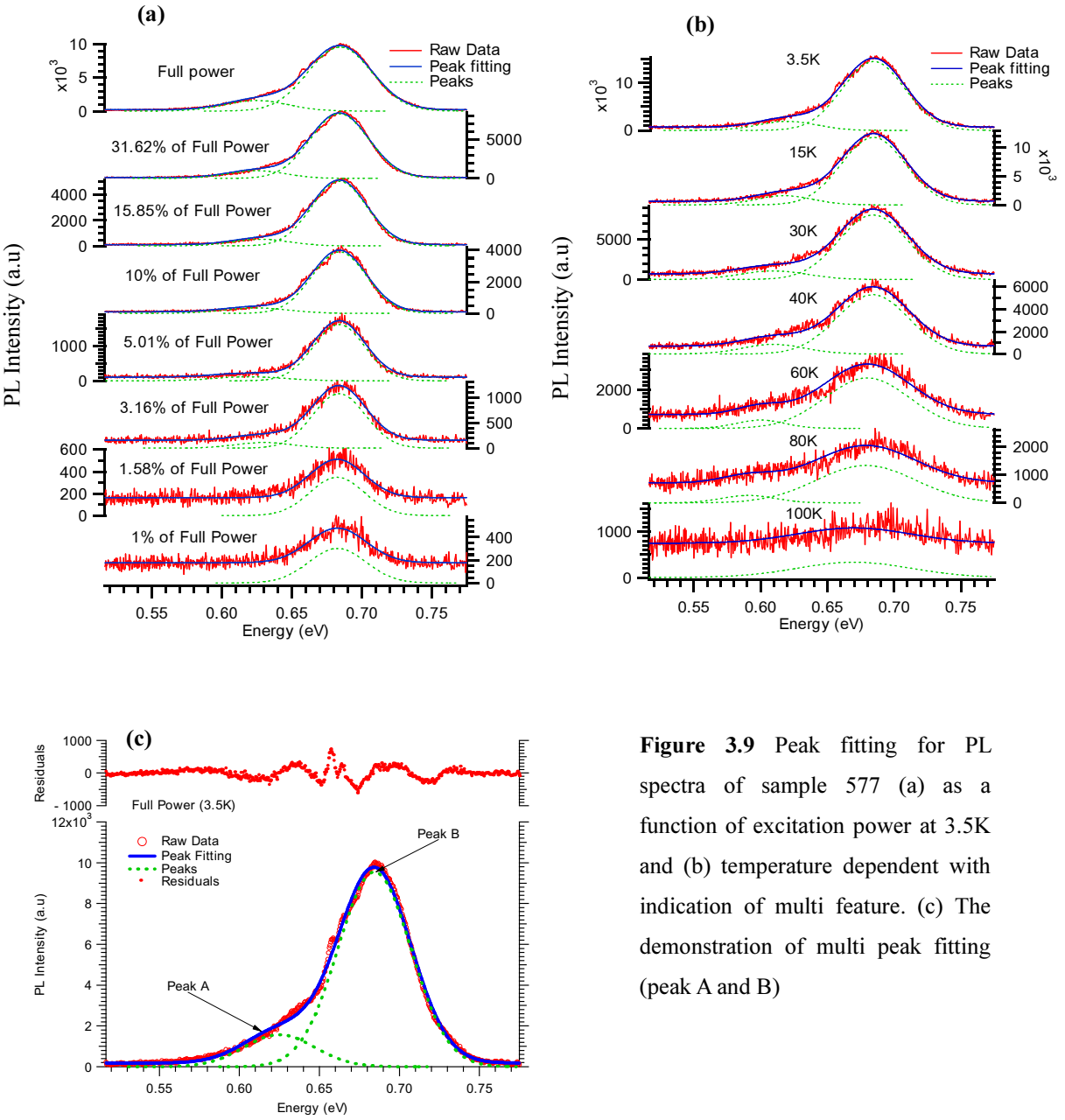

Figure 3.9 Peak fitting for PL spectra of sample 577 (a) as a function of excitation power at 3.5K and (b) temperature dependent with indication of multi feature. (c) The demonstration of multi peak fitting (peak A and B)

In order to evaluate the details of the features, the parameters of each peak have been displayed in figure 3.10 as function of power and temperature. The intensities of both peaks are constantly decreasing in proportion as a function of excitation power. However, above 30% of maximum power there is a very clear saturation of the intensity. The PL peak intensities versus excitation power have log slopes close to 1 indicating linear excitation processes of each peak [3]. The main PL emission (peak B) at 0.68 eV exhibits blueshift with increasing excitation power indicates prominent band filling effect at the top of the conduction band. Arnaudov *et al* explained that if the excitation intensity is high enough such

that the electron hole pair concentration becomes comparable with the free carrier concentration, peak shifting is expected [6]. However, the weaker peak A (0.63 eV) shows a scattered behaviour that is due to inaccuracies in the fitting process. This peak is significantly disturbed by the grating imperfection and thus its parameters are uncertain.

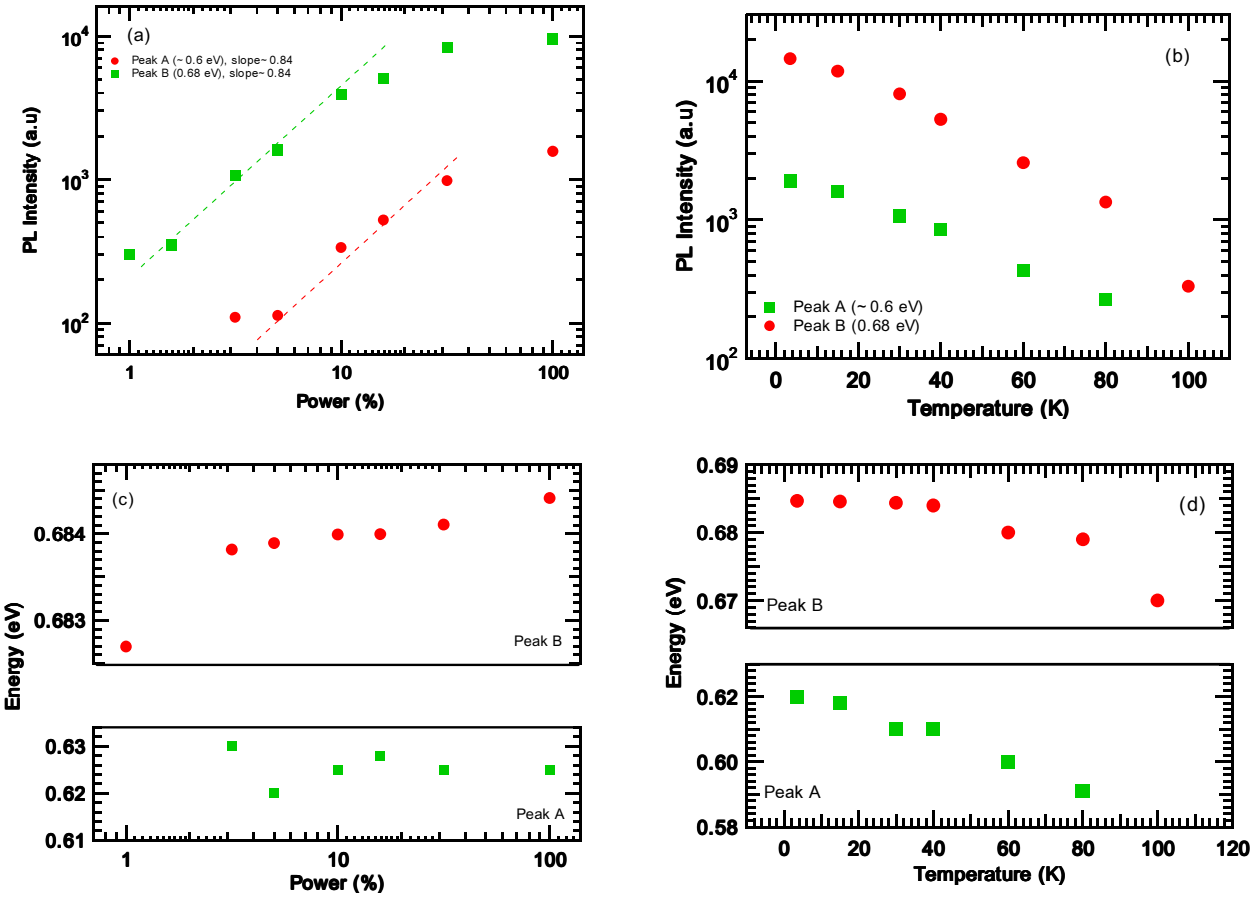

Figure 3.10 Peak intensities for two peaks (A and B) as (a) a function of excitation power (Fitted with straight line) and (b) as a function of Temperature. Location of the two major peaks (c) as a function excitation power and (d) as a function of temperature.

Meanwhile, the PL response as a function of temperature exhibits typical redshift with raised temperature. The spectral redshift with temperature is mainly influenced by thermal expansion which results in band gap shrinkage [4]. It is clearly depicted in figure 3.10 (d) that the two peaks redshifted approximately 20 meV as temperature increases. In a theoretical perspective, if the bandgap is between 0.67~0.69 eV, then the bandgap shrinkage for InN from liquid helium to room temperature should be restricted to 55~60 meV [7] which is

substantially weaker than in other group III-nitrides. For instance, under similar conditions the peak energy of GaN and AlN shift by about 72 and 92 meV [13]. The PL intensity of peak B (0.68 eV) exhibits relatively strong variability compared to peak A (~0.6 eV) as a function of temperature. The sensitivity of the PL spectrum to temperature shows that the population of one of two types of carriers forming the PL band is strongly related to temperature [2]. The intensity versus temperature data is analyzed later in this section using an Arrhenius model.

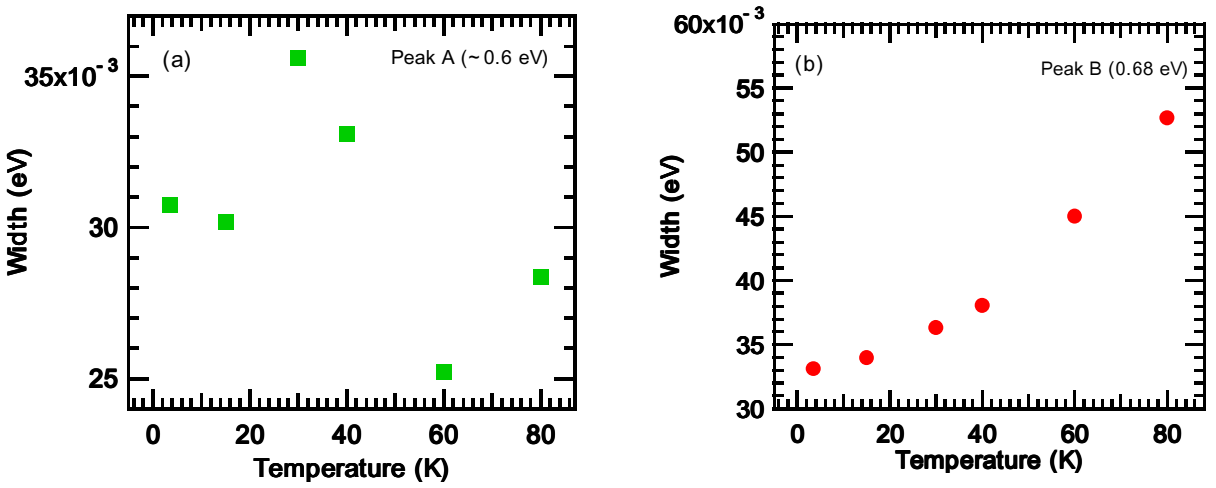

Figure 3.11 (a) The linewidth of peak A as a function of temperature shows no indication of any patterns. (b) Indication of typical broaden as temperature increase for peak B.

Furthermore, the PL line width as a function of temperature has been plotted in figure 3.11. The line width of peak B (0.68 eV) increased about 20 meV with increasing temperature which is dominated by longitudinal acoustic phonon scattering [7]. However, there was no indication of any patterns observed for linewidth of peak A (0.63 eV). Presumably, the parameters may not be certain due to insufficient PL signal for peak A.

Arrhenius plots of PL intensities at different temperatures are shown in figure 3.12. The commonly used model given by Ref. 12 is $I_{emis}(T)=I_0/1+C_1\exp(-E_1/kT)$ where E_1 is the activation energy, the coefficient C_1 measures the strength of the quenching process, I_0 represents the low temperature PL intensity and k is Boltzmann constant. The fits using this model are shown as the solid lines in figure 3.12. Adding a second activation energy such as $I_{emis}(T)=I_0/[1+C_1\exp(-E_1/kT)+C_2\exp(-E_2/kT)]$ results in a better fit as seen by the dotted line. This may be accounted for a possible existence of nonradiative recombination channels from Mg related emissions [5].

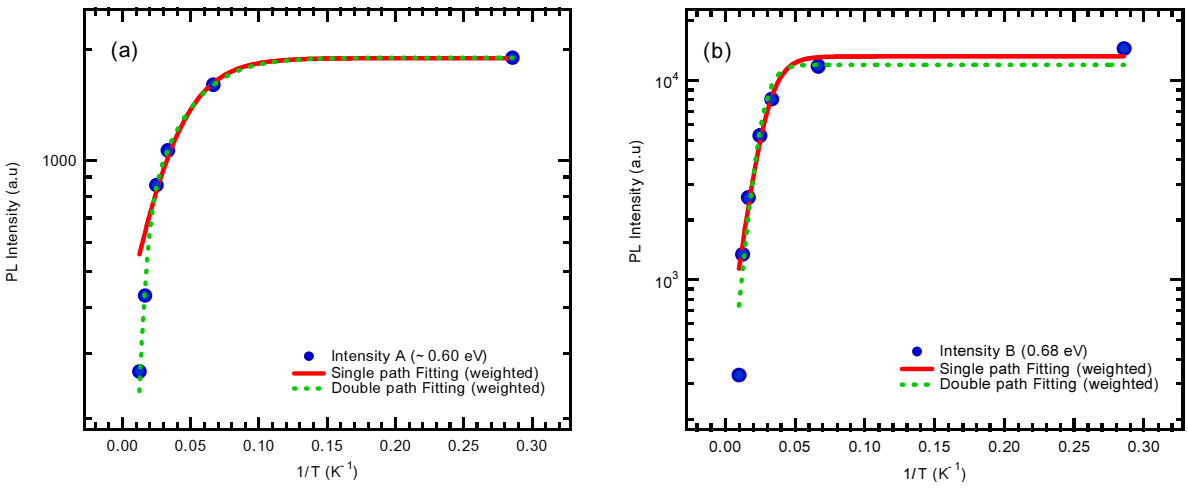

Figure 3.12. Arrhenius plots of the PL emission for (a) peak A (lower energy) and (b) peak B (higher energy)

Table 3.2. Activation energy and Arrhenius parameters of Peak A and B with single and double path

	χ^2	I_o	C_1	E_1 (meV)	C_2	E_2 (meV)
Single path (peak A)	5.15×10^6	1894±4	4.4±0.1	4.2±0.1		
Double path (peak A)	4.30×10^5	1894±4	160±250	24±9	3.7±0.3	3±1
Single path (peak B)	4.12×10^6	13200±700	40±30	11±2		
Double path (peak B)	4.01×10^5	12000±400	16400±400	14.6±0.2	15±1	80±40

As shown in table 3.2, the Arrhenius fit for peak B yields two activation energies of 15 and 80 meV. The best fit is obtained with a relatively small chi square value for peak A (double path) giving activation energies of 24 and 3 meV. No direct evidence of an Mg acceptor level in PL spectra was observed in sample 577. However, assumption that peak B is related to a transition from the conduction band to a Mg acceptor level would indicate a Mg acceptor level approximately 15 meV (E_1) above the valence band. The activation value E_2 for peak B is well coinciding with the spectral peak energy difference of about 80 meV between two peaks (A and B). However, determining the exact origin of the two activation energies still remains a formidable challenge.

Since the straight line slope of PL intensities as a function of excitation power yield less than 2 as shown in figure 3.10 (a), the transitions of peak A and B is most likely originated from Mg related levels as pointed out in Ref. 4. Also in considering the similar feature observed from Ref. 6 and the physical correlation between peak A and B as a function of temperature, the origin of peak A and B are estimated as the transition from deep and shallow acceptor levels, respectively. Despite, the PL emission of peak A had conflicting observations regarding peak shifting from power and temperature dependencies, these observations may be unsuited for the accurate estimation of the characteristics due to insufficient PL signal. By assuming the PL emission of peak A and B are Mg related emission, their activation energies (A ~24 meV, B ~15 meV) are fairly coincided well with calculated binding energy of a hydrogenlike acceptor 20 meV [6]. Thus the origin of peak A and B are considered as free electron transition to the deep and shallow acceptor states.

3.2.3 Sample 585: $Mg_{conc} = 6.2\times10^{17}$ cm^{-3}

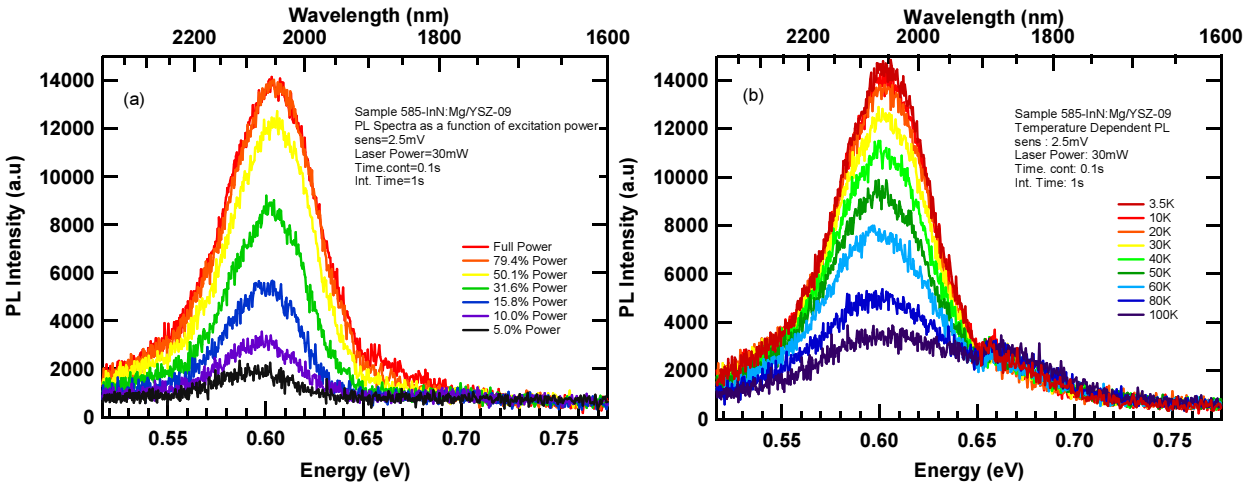

Figure 3.13. (a) PL spectra for sample 585-InN:Mg as a function of excitation power at 3.5K. (b) Temperature dependent PL for sample 585-InN:Mg with constant excitation power.

The sample 585-InN:Mg is expected to demonstrate strong PL feature due to its relatively low carrier concentration ~4.71×10^{18} cm^{-3} and high mobility ~295 cm^{-2}/Vs. Figure 3.13 displays PL spectra measured as functions of excitation power and temperature. The well resolved structure consisting three peaks in the energy interval from 0.5 to 0.7 eV was

observed. The main emission peak is centered at 0.6 eV, accompanied by two minor features at 0.54 and 0.67 eV. Unfortunately, the apparent dip observed in the PL spectrum at 0.65 eV is an absorption artifact that is thought to arise from OH vibrations present in the optical path.

It is worth noting that the dominant peak energy position exhibits a relatively low energy, approximately 80 meV less than previous films with low Mg concentrations. It can be attributed to relatively higher T_{Mg} when this sample was grown. Thus this may be influenced by partial effect of the position of a Mg acceptor state above valence band. Both data have been analyzed to peak fit individual lines to the spectra and the results of this fitting are displayed in figure 3.14 for excitation power and temperature variances.

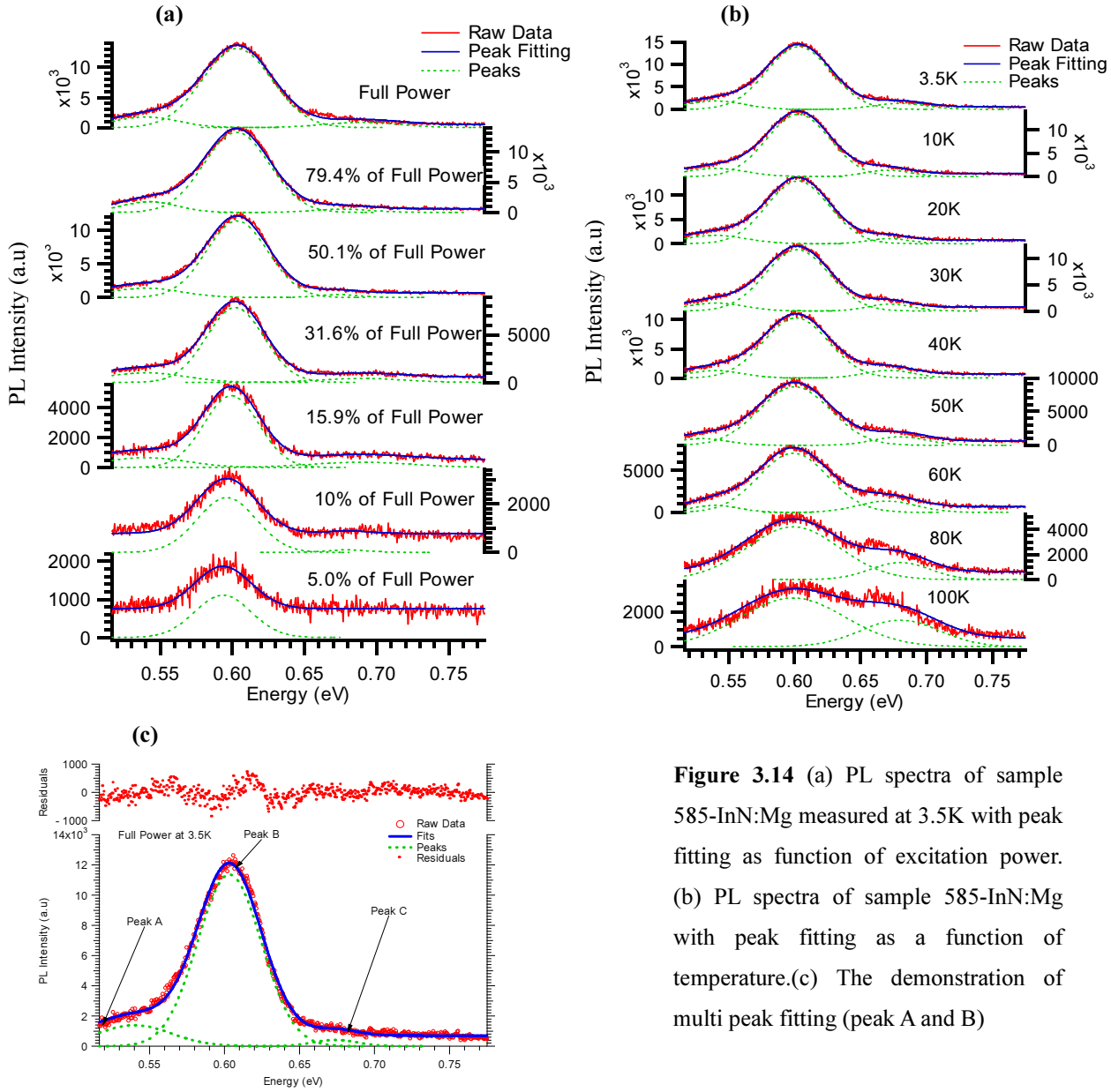

Figure 3.14 (a) PL spectra of sample 585-InN:Mg measured at 3.5K with peak fitting as function of excitation power. (b) PL spectra of sample 585-InN:Mg with peak fitting as a function of temperature.(c) The demonstration of multi peak fitting (peak A and B)

It is interesting to notice the minor peaks (A and B) at energy 0.54 and 0.67 eV disappeared at the low excitation power features where the signal is significantly broadened and noisy. Below 10% of full power, only a single symmetrical emission at 0.6 eV is detected. However, the PL behaviour of the sample with changing temperatures in figure 3.14 (b) is different from the power dependent feature. With increasing temperature, the peak energy of dominant peak eventually (peak B) merges with lower energy peak (peak A) and the higher energy shoulder near 0.67 eV becomes more apparent at high temperatures. The PL shape of the high energy wing has been changed effectively at high temperature due to inhomogeneous distribution of electrons [2]. V. Davydov *et al* also explained that the modification of the PL band shape with varying temperature as shown in figure 3.14 (b) is caused by the typical redshift in the energy levels in accordance with the Fermi function [7].

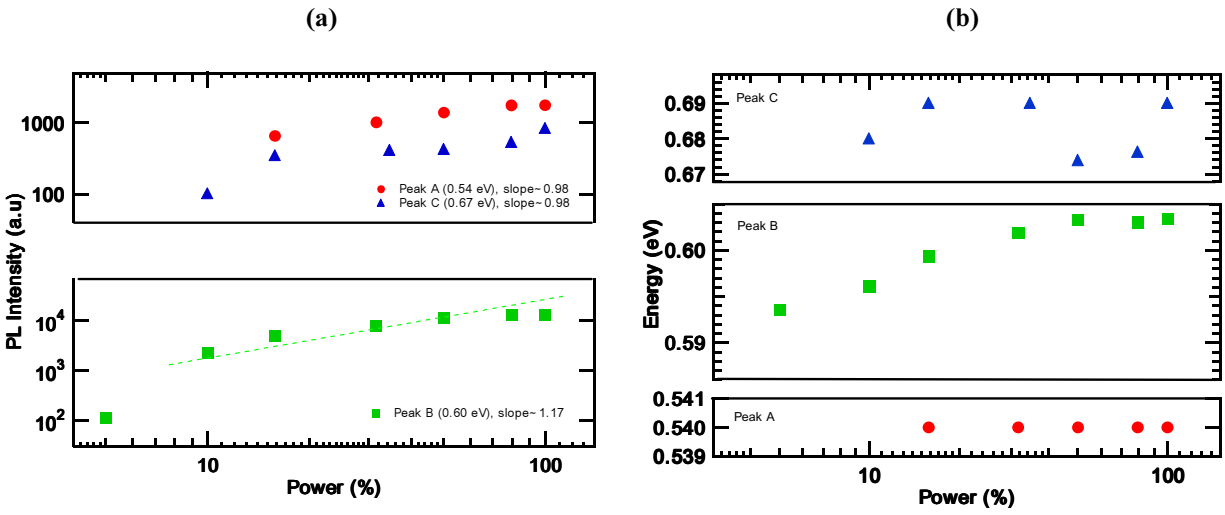

Figure 3.15 (a) The linear fits for intensity vs power (log to PL intensity and power). (b) The position of the peaks under different excitation powers.

Figure 3.15 (a) shows the PL intensities of the three peaks decrease by similar orders of magnitude with decreasing excitation power. The PL intensities of each peak as displayed in figure above, show a linear emission process for each peak. The peaks are likely related since the slopes of their peaks are very close. However, the linear independence of peak positions (3.15 (b)) show conflicting argument that there is no correlation between each peaks as a function of excitation power. The spectral blueshift has been observed for the dominant PL emission (peak B) possibly due to the band filling Burstein Moss effect. Another possible

explanation of this shift is suggested in Ref. 5 that at very high electron concentration the screening radius becomes smaller than the effective Bohr radius of holes. This leads to the non-equilibrium holes being pushed up over the recombination level in the valence band tails [5]. Meanwhile, the weaker peaks A (0.54 eV) and C (0.67 eV) show stabilized and scattered behaviours, respectively due to inaccuracies in the fitting process. These peaks are significantly affected by the grating imperfection and thus its parameters are uncertain.

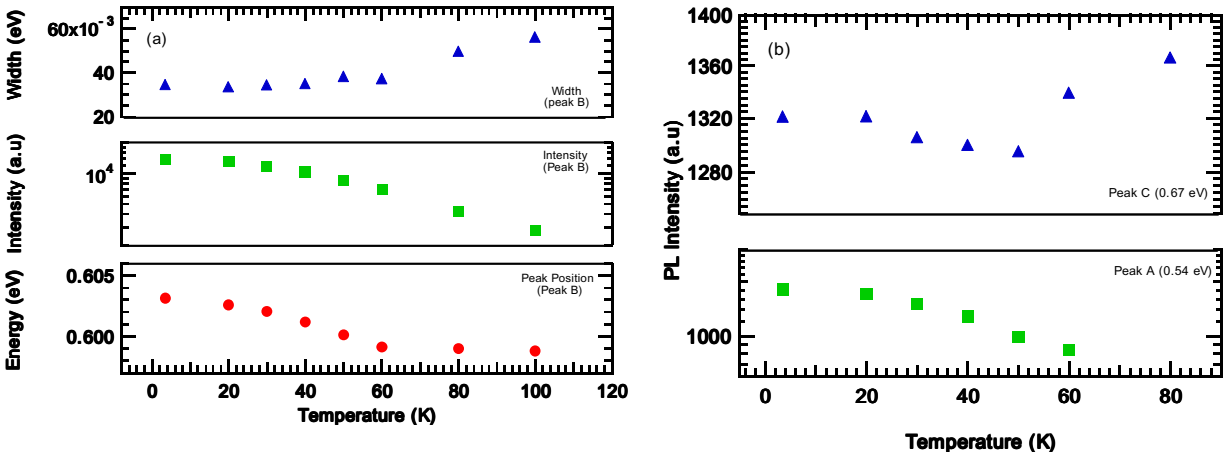

Figure 3.16 (a) Intensity, energy and line width of peak B (0.60 eV) as a function of temperature. (b) Energy of peak A and C as temperature changes.

To further explore the nature of each peak the parameters of each transition have been displayed in figure 3.16 as a function of temperature. Typical redshift and broadening of the PL band is clearly observed as temperature is increased for the dominant PL emission (peak B). In contrast to individual plots of power dependent features, the detailed plot as shown above gives evidence of a strong connection between peaks A (0.53 eV) and B (0.61 eV). The intensities of both peaks are constantly decreasing in the similar orders of magnitude as a function of temperature. However, the peak C (0.68 eV) shows anomalous behaviour in that its PL intensity increases in proportion to temperature above 50 K.

Varshni's fit for PL emission peak positions measured a different temperatures is shown in figure 3.17 (a). Eventually, the band gap of the main emission (peak B) is defined to be 0.603±0.001 eV at 0 K with the best fit. The peak energies above 80 K have been ignored due to insufficient PL signal. The experimental parameter values for β and α yield 983 K and 0.05 meV/K respectively. However, these values are not agree with the Varshni's parameters from Ref. 13, where β=454 K and α=0.41 meV/K.

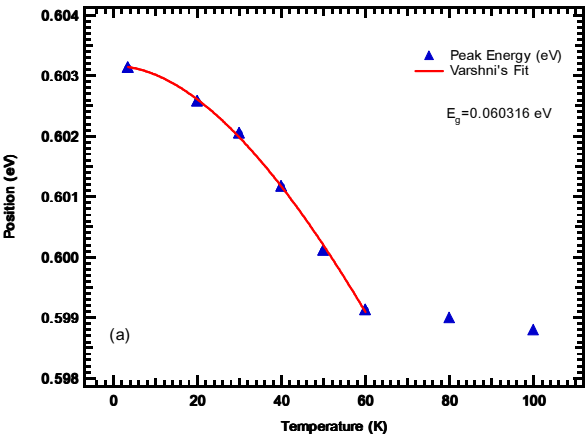

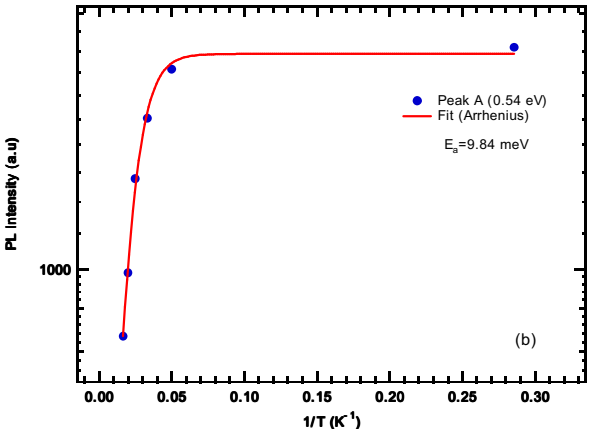

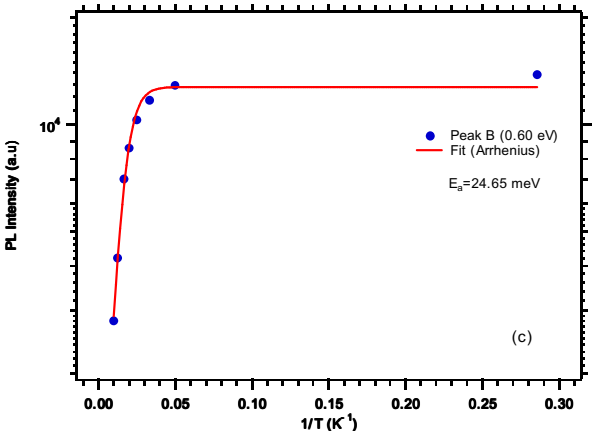

Figure 3.17 (a) Temperature dependent of PL peak B (At low temperature region 3.5 K ~ 60 K). Solid line represents the Varshni's equation. (b) The Arrhenius plots of peak intensities for peak A with weighted data. (c) The Arrhenius plots of peak intensities for Peak B with weighted data.

Table 3.3 The activation energy and Arrhenius fit for peak A and B with parameters

	χ^2	I_o	C_1	E_1 (meV)
Peak A	6131.83	1789.43±0.78	7.68±0.03	9.84±0.02
Peak B	3.02×10^6	12763±0.6	17.02±0.01	24.65±0.01

The Arrhenius plots for peak intensities A and B with different temperatures are shown in figure 3.17 (b) and (c). The high temperature data is weighted with the reciprocal of the intensity for the fits to accurately determine the activation energy. With a single activation energy, the model fits well and yields activation energies of 9.84±0.02 and 24.65±0.01 meV for peak A and peak B, respectively. Two activation energies for peak A and B may be accounted for by the existence of non-radiative recombination channels as suggested in Ref 12.

In previous investigation on GaN, it was reported as acting as semi-insulating with Mg dopant [8,9,10]. In similar trend with InN, it can be illustrated that the transition of dominant peak (peak B) is most likely from Mg related states (free to bound). By comparing the features from sample 577 and 579, the deep acceptor states indicate near energy of 0.6 eV. Also the fitting result of the activation energy for peak B (~25 meV) is in very good agreement with the binding energy of deep acceptor state from sample 577 (peak A ~ E_I= 24 meV)*. The energy position of peak A (0.54 eV) is in strong correlation with peak B in temperature variations and agrees well with the data of Ref. 2. Therefore, it can be regarded as a manifestation of the electron and phonon interaction (the phonon replica of the band, due to deep acceptors) [2]. Theoretically, it is insufficient to estimate peak A as a donor acceptor pair transition since no significant blueshift was observed with increasing excitation power. Finally, as depicted in figure 3.16 (b), peak C (0.68 eV) exhibits no relative variability with temperature variations. Therefore, it can be assumed tentatively that the origin of peak C may be the transition from free exciton state.

4.2.4 Sample 555: $Mg_{conc}=8.7\times10^{17}$ cm^{-3}

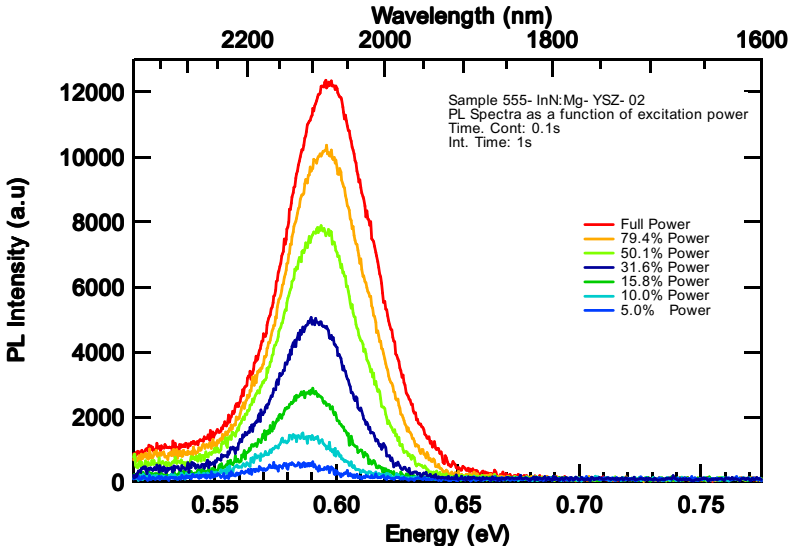

Figure 3.18 PL spectra of sample 555-InN:Mg as a function of laser power at 3.5K. The graph is normalized with magnitude of intensity 10mV Lock-in sensitivity (full laser power ~30mW)

Sample 555-InN:Mg exhibits one of the strongest PL emission compared to any other Mg doped InN samples. The T_{Mg} for sample 555 was relatively high ~225 ˚C. As shown in

* See table 3.2

figure 3.18, a strong emission peak was detected using a Lock-in sensitivity of 10mV. The single symmetrical emission peak is located at 0.59 eV and below 80% of full laser power the small peak at ~0.55 eV was not detected as displayed in figure 3.19 (a). The presence of a blueshift with increasing excitation power known as the Burstein-Moss effect was clearly observed. The logarithm PL intensities of a main emission peak as displayed in figure 3.19 (b) shows a linear emission process (slope of straight line fit yields close to 1). The linewidth at the highest power is noticeably broader than at low. This is likely due to heating of the sample from the laser as excitation intensity increases.

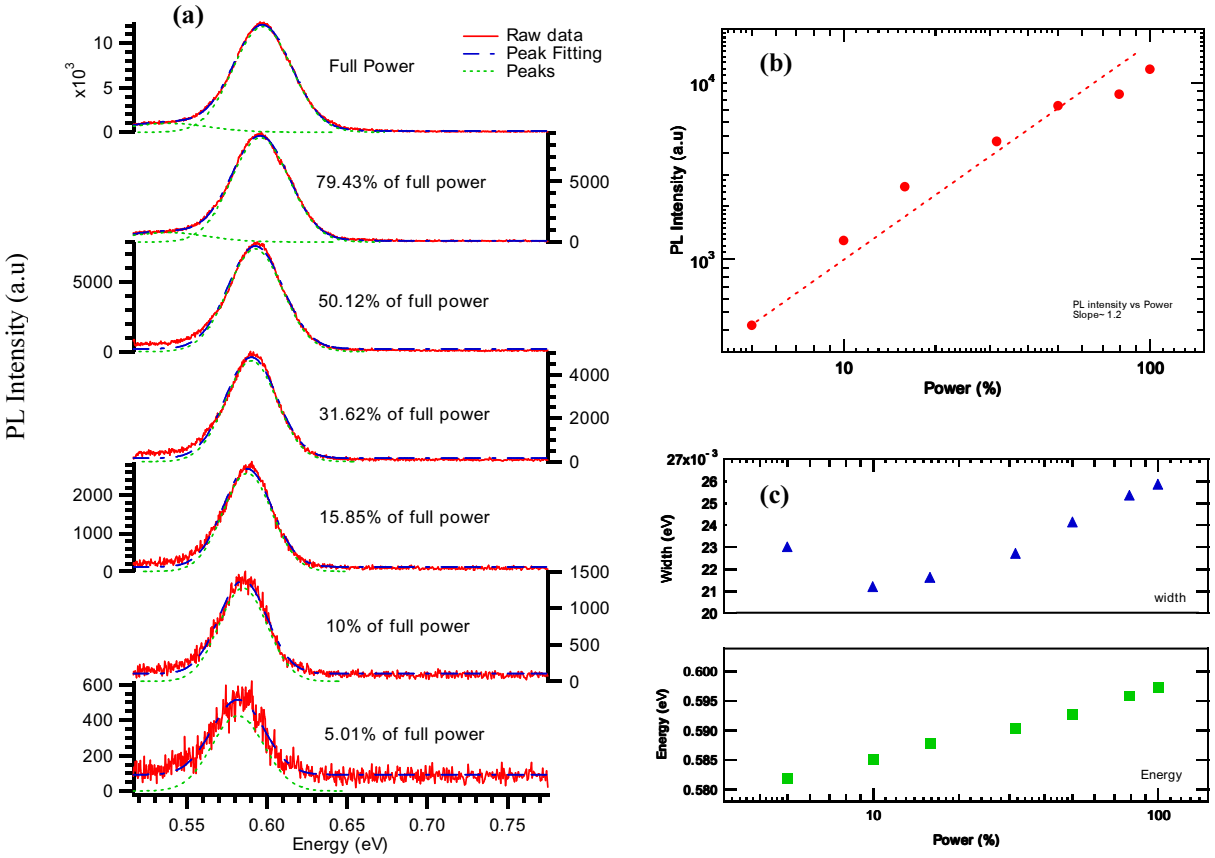

Figure 3.19 (a) 3.5 K PL spectra of 555-InN:Mg as a function of power with peak fitting. (b) PL intensity (straight line fit) as a function of power. (c) Energy and linewidth of PL vs power.

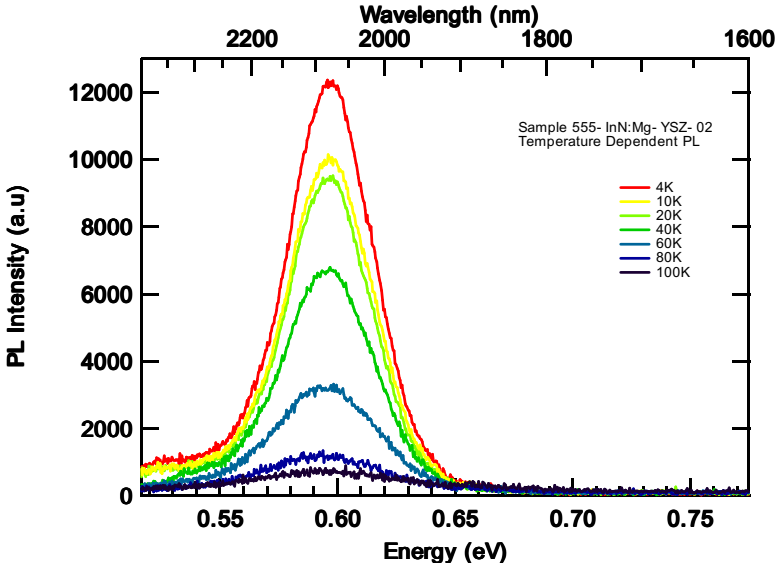

Figure 3.20 Temperature dependent PL for sample 555-InN:Mg with constant excitation power (30 mW). The magnitude of intensity is 10 mV Lock-in sensitivity with 1s integration time and 0.1s time constant..

The temperature dependent PL spectra exhibit typical behaviour in the range from 3.5 K to 100 K. A redshift was observed with increasing temperature along with a relatively rapid decay of the intensity from 20 K. The slope of high energy wings of the PL is affected by temperature as the PL band shapes are potentially influenced by the inhomogeneous distribution of electrons [2].

The temperature dependent PL behaviour of sample 555-InN:Mg in figure 3.21 (a) shows the appearances of a minor peak at the high energy side (~0.68 eV) of the main peak as temperature increased. In considering the similarity between the emission spectrum of the sample 585 [see figure 3.14(b)], structures consisting of two features at high temperature (100K) can be understood in a similar trend. Two peaks can be illustrated as the deep acceptor and free exciton features, respectively for origin of peaks at energy 0.60 and 0.68 eV.

Figure 3.21 (b) shows a detailed experimental summary for sample 555. Consistent with previous temperature dependent PL, intensity, the peak position and linewidth were drastically affected by temperature. The change in PL intensity as a function of temperature indicates the enhancement of nonradiative processes [2]. The typical redshift is observed where the PL band position is affected as temperature increases, by bandgap shrinkage. It is interesting notice that the magnitude of the redshift of PL peak energy in this sample is significantly weaker than that in previous InN:Mg films. Probable reason is more free electrons thermalized from defects or impurities in this sample can fill the conduction band and

compensate the effects of the bandgap shrinkage with temperature [4]. Furthermore, the linewidth of dominant peak increased approximately 20 meV with increasing temperature which is dominated by longitudinal acoustic phonon scattering [7].

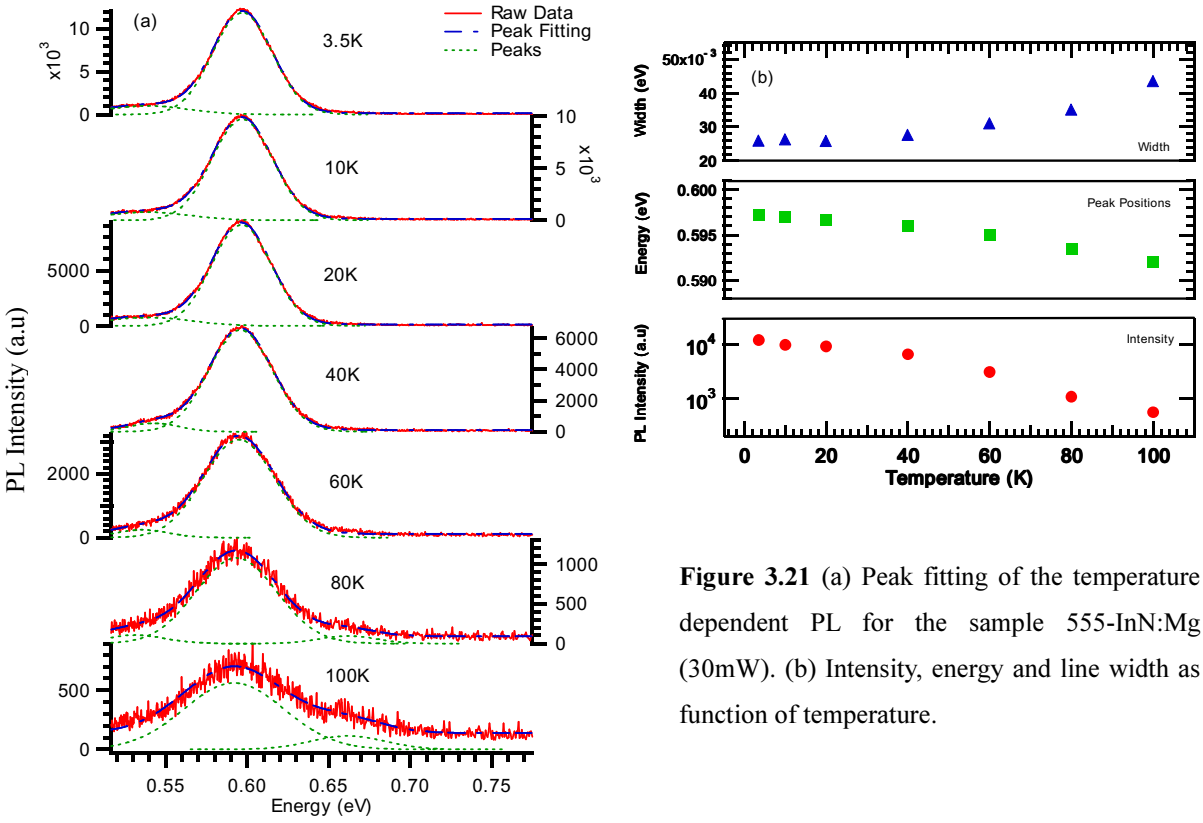

Figure 3.21 (a) Peak fitting of the temperature dependent PL for the sample 555-InN:Mg (30mW). (b) Intensity, energy and line width as function of temperature.

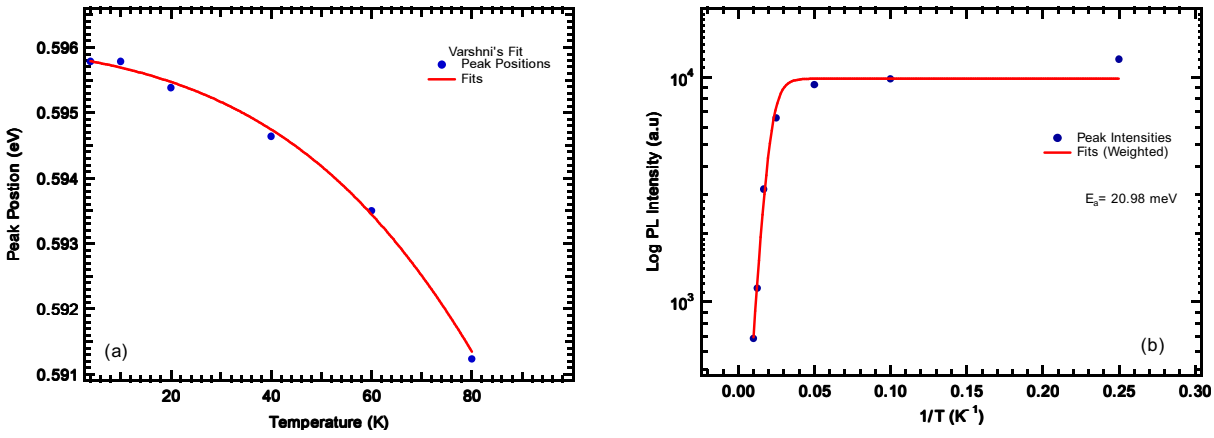

Figure 3.22 (a) Temperature dependent of PL peak position of the sample 555-InN:Mg. The solid line represents the Varshni's equation. (b) The Arrhenius plots of peak intensities for the sample 555-InN:Mg. The solid line is the one activation energy fit when the high temperature data is weighted more heavily.

For further detail, the pronounced redshift of the dominant PL peak is characterized by Varshni's equation ($E(T)=E(0)-\alpha T^2/(T+\beta)$) in figure 3.22 (a). The location of this peak at the lowest temperature is at relatively low energy, 0.59 eV, which may be the result of the degenerate band to "pushed up" tails in valence band by effective high Mg concentration [6]. The experimental parameters for β and α yielded 841 K and 0.03 meV/K, respectively which are fairly consist with the Varshni's parameters from sample 585-InN:Mg.

The Arrhenius plot along with the one activation energy fit is displayed in figure 3.22 (b). An activation energy of 20.98±0.01 meV is obtained when the high temperature data is more heavily weighted (reciprocal of the intensity) in the fit. It is worth noting that the lower activation energies are often observed in heavily doped samples due to screening, as with Mg in GaN [14]. The parameters for I_o and C_1 yield 9837.89±0.46 and 150.21±0.03, respectively. The lowest temperature data point has been ignored in the fit to more precisely follow the slope in the high temperature region. The single activation energy fits the data reasonably well and so a second activation energy was not included. The fitting result of the activation energy (~21 meV) is coincided well with deep acceptor binding energies from previous InN:Mg samples (585 ~25 meV and 577 ~24 meV). Thus, by assuming the peak B is originated from the deep acceptor transition, the activation energy indicates Mg related acceptor level is placed 21 meV above the valence band.

3.3 References

[1] X. Wang, S.B. Che, Y. Ishitani and A. Yoshikawa, Appl. Phys. Lett. **90**, 201913 (2007)

[2] A. A. Klochikhin, V. Yu. Davydov, V. V. Emtsev, A. V. Sakharov, and V. A. Kapitonov, Physical Review B **71**, 195207 (2005)

[3] T. Schmidt, K. Lischka and W. Zulehner, Phys Review B **45**, 16 (1992)

[4] Fei Chen, A. N. Cartwright, Hai Lu, William J. Schaff, Physica E **20** (2004) 308-312

[5] G. W. Shu, P. F. Wu, M. H. Lo, J. L. Shen, T. Y. Lin, H. J. Chang, Y. F. Chen, C. F. Shih, C. A. Chang, and N. C. Chen, Appl. Phys. Lett. **89**, 131913 (2006)

[6] B. Arnaudov, T. Paskova, P. P. Paskov, B. Magusson, E. Valcheva, and B. Monemar, H. Lu, W. J. Schaff, H. Amano and I. Akasaki, Phys Review B **69**, 115216 (2004)

[7] V. Yu. Davydov, A. A. Klochikhin, V. V. Emtsev, D. A. Kurdyukov, S. V. Ivanov, V. A. Vekshin, F. Bechstedt, J. Furthmuller, J. Aderhold, J. Graul, A. V. Mudryi, H. Harima, A. Hashimoto, A. Yamamoto, and E. E. Haller, Phys. Stat. Sol (b) **234**, No. 3, 787-795 (2002)

[8] G. Pozina, B. Monemar, P. Paskov. Physica B Condensed Matter 40, 302-306 (2007)

[9] M. K. Kwon, I. K. Park, J. Y. Kim, J. O. Kim, B. Kim, S. J. Park. IEEE Photoics Technology Lett 19, 1880-1882

[10] T. Eberlein, R.Jones, S. Oberg, D. Briddon Appl Phys Lett 91, 32105 (2007)

[12] N. Khan, N. Nepal, A. Sedhain, J. Y. Lin, and H. X. Jiang, Appl. Phys. Lett. **91**, 012101 (2007)

[13] W. Walukiewicz, S.X. Li, J. Wu, K.M. Yu, J.W. Ager III, E.E. Haller, Hai Lu, William J. Schaff, Journal of Crystal Growth **269** (2004) 119-127

[14] P.A. Anderson, C. H. Swartz, D, Carder, R. J. Reeves, and S. M. Durbin, Appl. Phys. Lett **89**, 183104 (2006)

Chapter 4 Results of Zn doped InN

4.1 Introduction

Despite observable PL from lightly Mg doped InN, some anomalous phenomena resulting in PL quenching in p-type samples remains a formidable challenge to overcome. For further interpretation of the fundamental properties of p-type InN, zinc (Zn) has been recommended for the next candidate as a p-type dopant. Considering the several similarities between InN and InAs, Zn might presumably be a viable dopant for InN [1]. As this was the first attempt to demonstrate evidence of Zn acceptors in InN, determining Zn doped InN required comprehensive practical investigation. A precise study of Zn doped InN may allow for a reliable comparison of Mg and Zn doped InN.

In this chapter, the fundamental properties of p-type InN will be explored with a series of Zn doped InN samples. Similar to InN:Mg, InN:Zn samples were grown locally at University of Canterbury using a conventional plasma-assisted molecular beam epitaxy (PAMBE) system. Films were grown on sapphire substrates and more latterly YSZ substrates that had a GaN template deposited by metal organic chemical vapour deposition (MOCVD). PL emission from the InN:Zn samples was analysed by a small spectrometer (Minimate) and an InSb detector. The general properties such as the emission shape and peak energy have been analyzed comprehensively by the Igor computer package. In some cases an Ar^+ laser was used as the excitation source to increase the PL signal.

4.2 Results of Individual Samples

The purpose of this investigation was to supply plausible evidence that Zn doped InN is capable of light emission. The initial series of films were grown under N-rich conditions and had Zn cell temperatures from 60-248 ˚C. It transpired that PL was detectable only for films with low cell temperatures and thus presumably light Zn doping. Therefore, considering several similarities between InN and GaN a new series of InN:Zn films were grown under an In-rich condition. In a previous report, a Ga-rich condition was preferable for efficient dopant incorporation in GaN [2]. Under In-rich conditions, several prominent PL features were pronounced in the InN:Zn samples with significantly high PL intensity. Table 4.1 shows the growth conditions of each sample which has been produced for this research. In order to describe the optical characteristics of Zn doped InN, each sample's PL behaviour will be analyzed individually. Further work is necessary to uncover the origin of PL quenching in highly doped material. However, evidence from the strong PL from lightly Zn-doped InN shows Zn may be a viable acceptor for InN.

Table 4.1: The table of Zn-doped InN Samples produced by Electrical and Computer Engineering Department.

Sample Number	Zn temp (˚C)	PL	Ar^+ Laser Power (mW)	Carrier Concentration (cm^{-3})	Hall Mobility (cm^{-2}/Vs)
634-InN:Zn/YSZ	60	Yes	62 (diode)	1.73×10^{19}	944
617-InN:Zn/YSZ	75	Yes	730	-	-
615-InN:Zn/YSZ	100	No	800	1.67×10^{19}	44
604-InN:Zn/YSZ	114	No	800	9.21×10^{18}	114
611-InN:Zn/YSZ	127	No	800	1.17×10^{19}	149
610-InN:Zn/YSZ	143	No	800	2.28×10^{19}	100
613-InN:Zn/YSZ	192	No	800	4.14×10^{18}	68
612-InN:Zn/YSZ	248	No	800	2.47×10^{19}	98
*656-InN:Zn/GaN	75	Yes	150	9.00×10^{18}	540
*653-InN:Zn/GaN	192	Yes	150	3.80×10^{18}	700
*655-InN:Zn/GaN	248	Yes	150	5.00×10^{18}	370

Note: * indicates the samples grown under In-rich conditions (relatively high mobility).

4.2.1 Sample 617

Sample 617-InN:Zn was the first film to produce the detectable PL emission. Despite insufficient PL signal to provide direct evidence of acceptor-related luminescence, it shows luminescence may eventually be observed from p-type Zn doped InN. To achieve resolvable PL spectra, the excitation source was enhanced up to 730mW. As shown in figure 4.1, the film with Zn cell temperature of (T_{Zn}) ~75 ˚C exhibits a relatively low peak energy at 0.59 eV with a linewidth of about 100 meV.

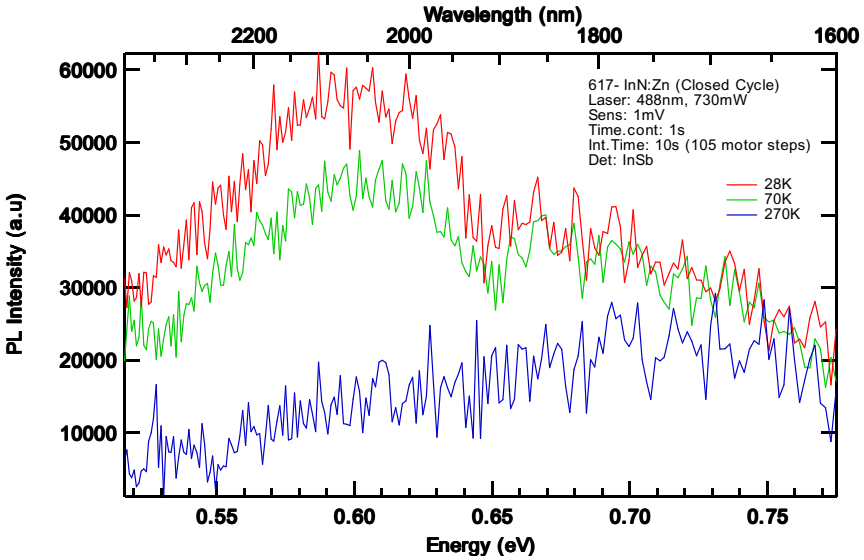

Figure 4.1 PL spectra of sample 617-InN:Zn at various temperatures (Closed cycle system with 10 times longer integration time).

By assuming the PL spectra of 617-InN:Zn contains the transition from a Zn acceptor level, the PL emission peak centered at 0.6 eV is originated from deep acceptor state. This estimation is made since the deep and shallow acceptor transitions were determined at 0.6 and 0.68 eV, respectively for Mg doped InN. However, it has still yet to be confirmed that Zn has an illustrated potential as p-type dopant. For comprehensive research on Zn doped InN, consecutive PL behaviour under different circumstances will be discussed in the following sections.

4.2.2 Sample 634 (N-Rich)

The sample 634-InN:Zn was grown with relatively low T_{Zn} of 60 ˚C. The PL signal of this film as a function of excitation power is shown in figure 4.2. A strong PL emission was observed throughout the experiment. The dominant peak was located at 0.67 eV and its peak energy exhibits prominent blue shift as a function of excitation power, possibly due to the Burstein-Moss effect. The total spectra consist of several peaks which are sensitive to the excitation power.

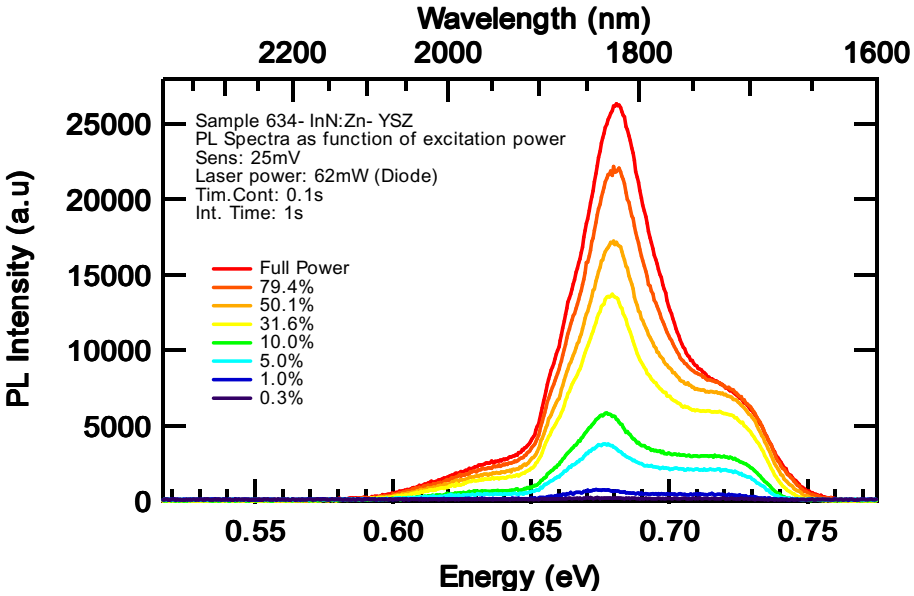

Figure 4.2 Variation of the PL spectrum of sample 634-InN:Zn with the excitation power at 3.5K. The spectrum was detected by InSb detector with the 532nm line of the laser diode as the excitation source.

Figure 4.3 (a) depicts the PL spectra as a function of excitation power along with multi peak fits. The spectra are composed of four Gaussian peaks labelled A~D as shown in figure 4.3 (b). It is worth noting that from the highest to the lowest excitation power a redistribution of intensities between two higher energy peaks (peak C and D) is observed. It may be influenced by the saturation of localized states by electron- hole pairs and the equilibrium distribution of holes which is established [3]. A logarithmic plot of integrated intensities at various excitation powers is depicted in figure 4.3 (c) with most peaks drastically depending on excitation power. Above 50 % of maximum power there are very clear saturation of the intensities for peak C (0.70 eV) and D (0.72 eV). The straight line fits for each plot yields a slope close to 1 for all three peaks and this is typical for transitions in direct bandgap semiconductors [3] but these are not shown in the figure for clarity.

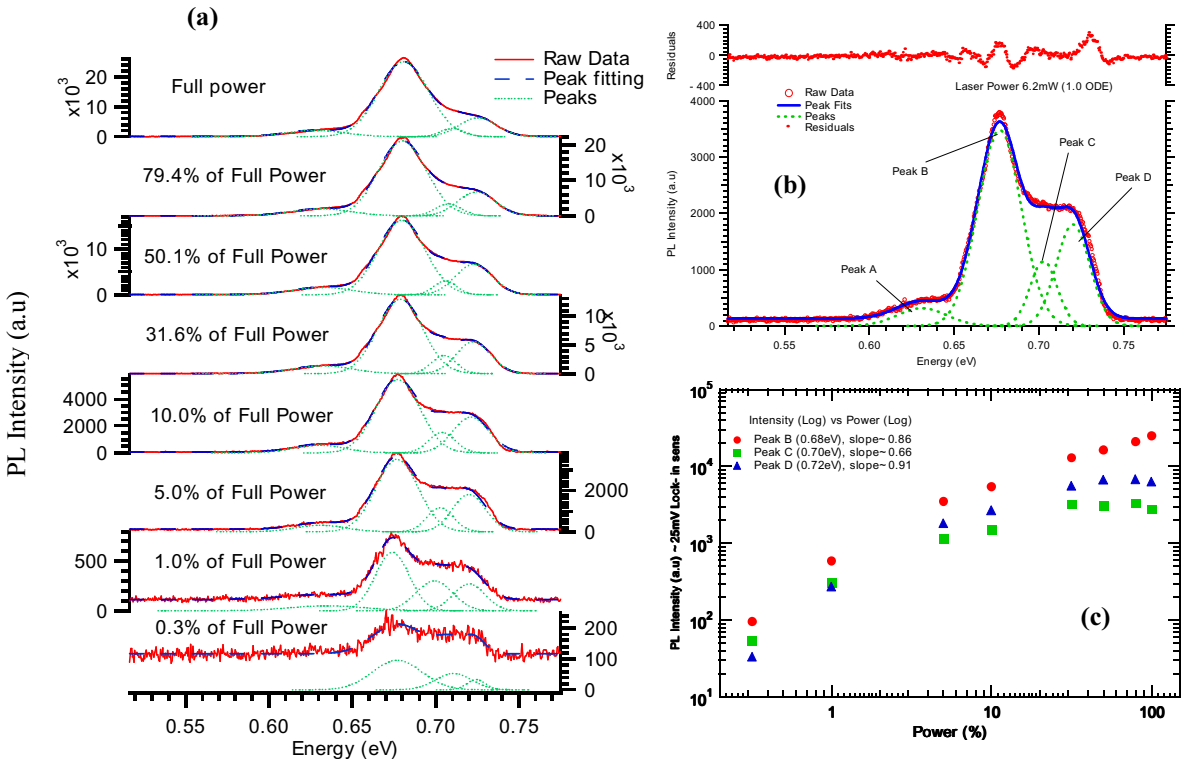

Figure 4.3 (a) The PL spectra of sample 634-InN:Zn as a function of excitation power with peak fitting. (b) Demonstration of peak fitting at 6.2mW excitation power. (c) The PL peak integrated intensities for peak B, C and D as a function of excitation power. Slope of each transition yield 0.91 (peak B), 0.66 (peak C) and 0.86 (peak D)

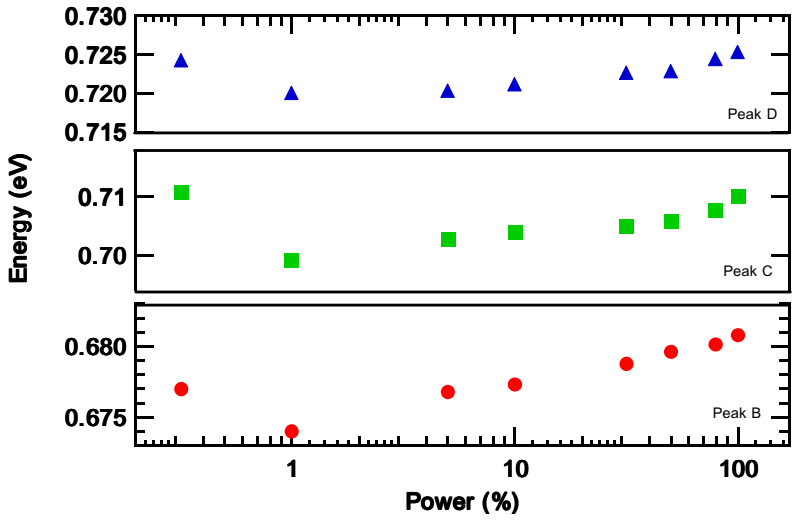

Figure 4.4 Peak energy positions as function of excitation power.

Note: The sudden redshift at the lowest excitation power may be influenced by the difficulty in defining the peak center due to relatively weak and noisy PL signal.

The prominent blue shifting as excitation power increases is observed as shown in figure 4.4. This may indicate a band filling effect influenced by the induced photocarriers [4]. Peaks B, C and D tend to shift in the same proportion that the difference between the highest and the

lowest energy is approximately 10 meV. The sudden redshift at the lowest excitation power may be influenced by the difficulty in defining the peak center due to relatively weak and noisy PL signal. Thus, determining the fundamental properties and origin of each feature at low excitation powers are rather ambiguous.

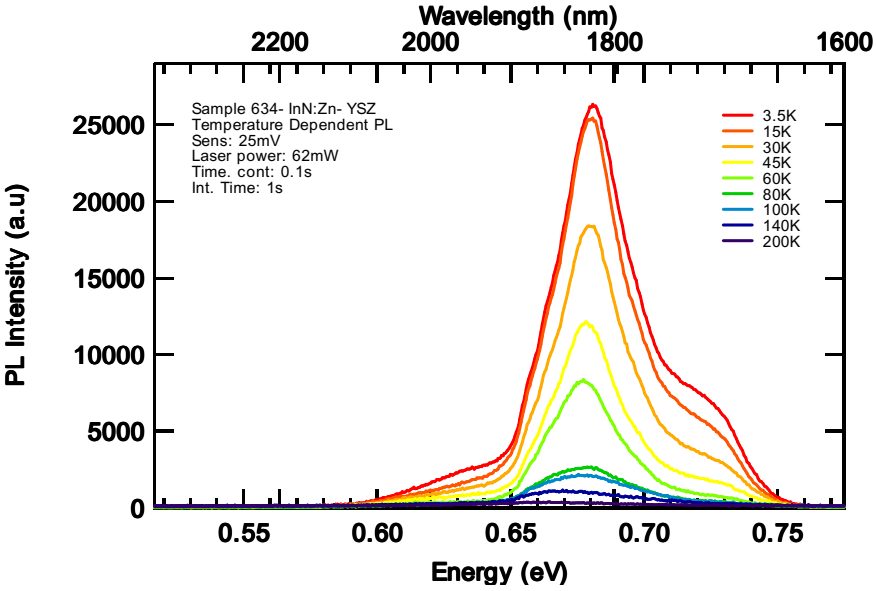

Figure 4.5 PL spectra for sample 634-InN:Zn as a function of temperature at constant excitation power.

It is a very difficult job to determine the origin of peaks based only off of power dependent measurements. A reasonable requirement for further understanding of the features would be a temperature dependent study. In order to quantitatively assess the observed peaks and their agreement with the proposed interpretation, temperature dependent PL was carried out. Figure 4.5 shows the temperature dependent PL from 3.5 to 200K.

The temperature dependent data has been analysed to peak fit individual lines to the spectra and the results of this fittings are displayed in figure 4.6. The multi peak fitting is showing three peaks labelled A (0.63 eV), B (0.68 eV) and D (0.72 eV). It is interesting to note that there is no indication of PL emission at 0.7 eV (peak C) as a function of temperature. With increasing temperature, the dominant emission peak energy (peak B ~0.68 eV) exhibits typical redshift and finally merges with the other transitions (peak A ~0.63 eV and D ~0.72 eV). This phenomenon may be attributed to thermal ionization of electrons and holes in donor and acceptor states [5]. The peak intensities of each emission are constantly decreasing in proportion to each other without any indication of saturation as shown in figure 4.6 (c).

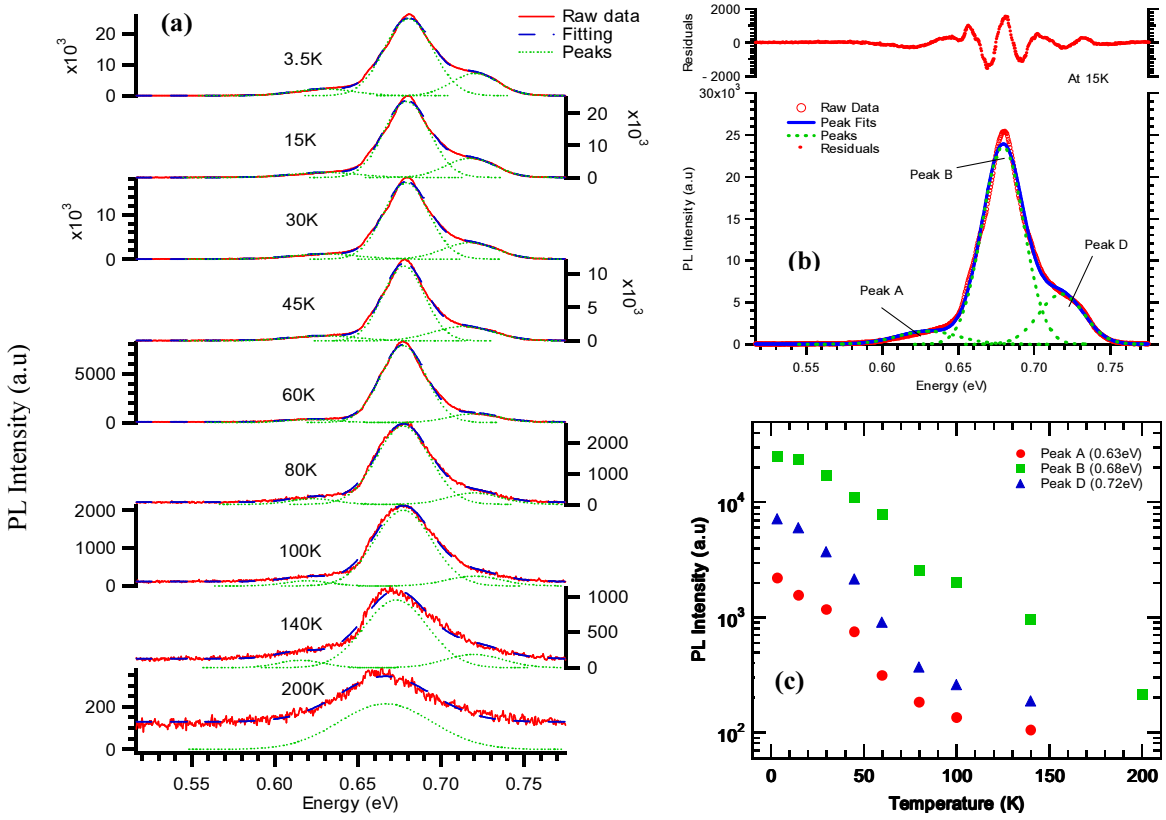

Figure 4.6 (a) PL spectra of sample 634-InN:Zn as a function of temperature with peak fitting. (b) Demonstration of the peak fitting at 15K with constant excitation power ~62mW (no indication of peak C at 0.7eV). (c) PL peak intensities for peak A, B and C as function of temperature.

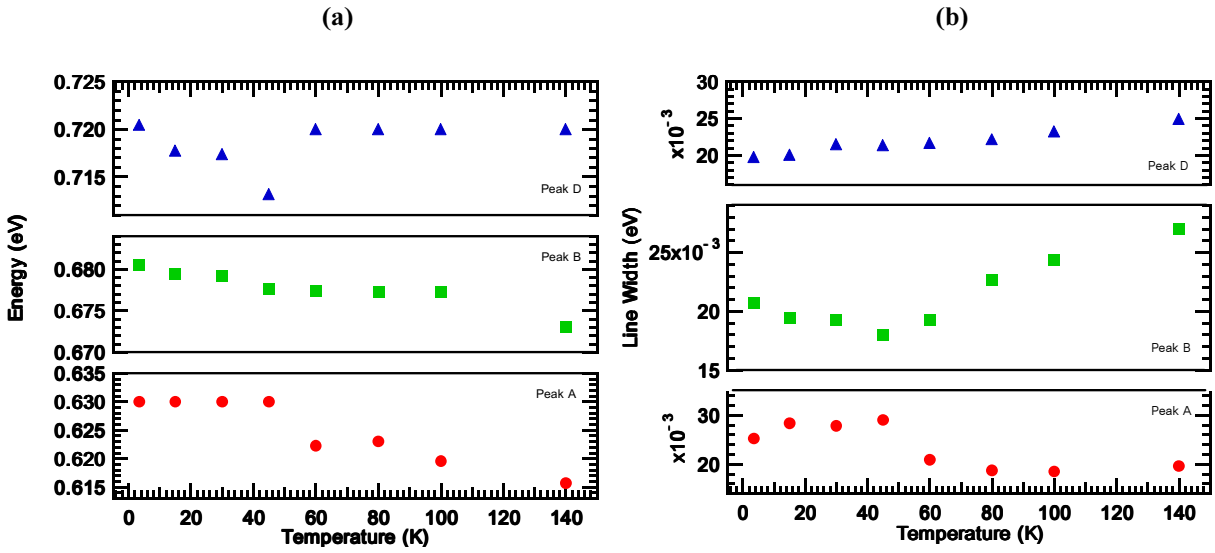

Figure 4.7 (a) Peak positions as a function of temperature for three features A, B and D. (b) Variation of the linewidth as a function of temperature.

Figure 4.7 summarizes the change in peak energies and linewidth with respect to temperature. For peak B (0.68eV), the emission energy shows a small shift as a function of temperature. The redshift in direct band gap semiconductors is attributed to the relaxation of the crystal lattice spacing. The difference between the maximum and minimum energy is only 3 meV indicating the amount of bandgap shrinkage as a function of temperature is less than usual. Rarely, the PL peak shifts to larger energies such as peak D at 60 K. This can occur depending on the type of strain induced in the material. The linewidth of the shallow acceptor transition emission line (peak B) initially decreases with increasing temperature up to 60 K but it tends to broaden due to longitudinal acoustic phonon scattering.

It is worth noting that, the linewidth of excitonic features should gradually increase with temperature by acoustic phonon scattering [4]. The linewidth broadening of excitons due to the exciton–phonon interaction gives $\Gamma(T) = \Gamma(0) + A_1 T + \Gamma_{ep} / [\exp(\Theta_{Lo} / T) - 1]$. The first term in this expression represents the broadening invoked from temperature-independent mechanisms, such as impurity, dislocation and surface scattering, electron interaction and Auger processes. The second term is the contribution from acoustic phonon scattering. The last term is caused by the exciton-LO phonon interaction. According to figure 4.7 (b), peak D is most likely related with the empirical broadening equation of excitonic features.

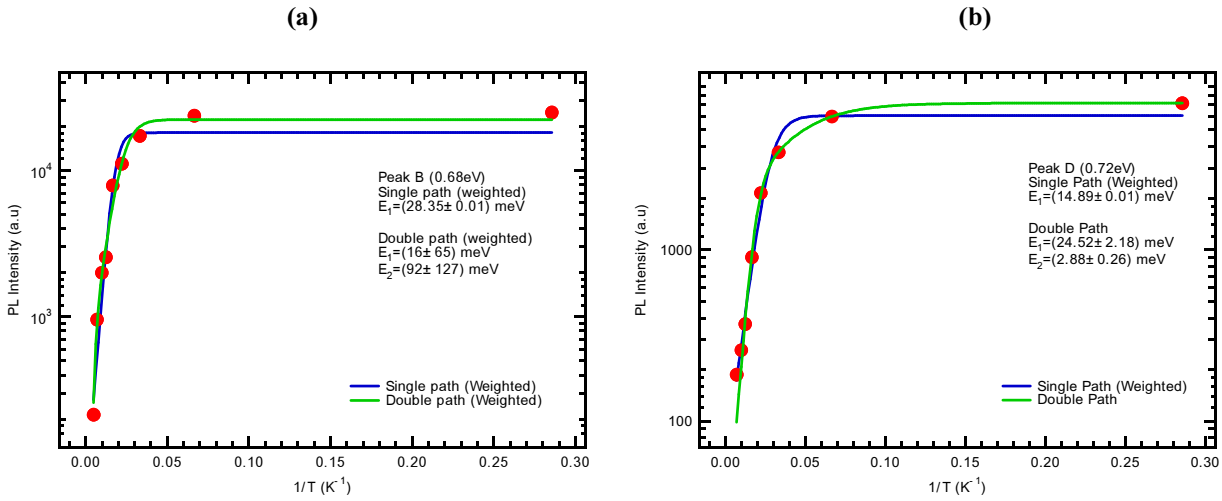

Figure 4.8 Arrhenius plots of the integrated PL intensities for (a) Peak B and (b) Peak D within comparison between single and double activation energy fits using weighted fitting

Finally, the Arrhenius plots of integrated PL intensities for sample 634-InN:Zn is displayed in figure 4.8. For the single path weighted fit activation energies of 28 and 15 meV, are obtained for peak B and D, respectively. The activation energies for the single path fit are higher than expected and may be attributed to the existence of an additional non-radiative recombination channel [6].

It is clearly observed from the figures above, that the double path activation energy fits better the than single path fit showing relatively low chi square values. The fitting results in activation energies of 16 and 92 meV for E_1 and E_2, respectively for peak B. They represent the thermal activation energy in high and low temperature regions. The value E_1 is reasonably close to the localization energy due to potential fluctuations caused by randomly located ionized impurities [7]. The high activation energy in the high temperature region E_2, indicates high efficiency luminescence which is attributed to a low concentration of trapping centers in the crystal [5]. Also in a similar fashion, the thermal activation energies for peak D are 25 and 2.9 meV for high and low temperature region, respectively. The Arrhenius parameters with uncertainties are shown in table 4.2.

Table 4.2 Activation energies and Arrhenius parameters of Peak B and D with single and double path fits.

	χ^2	I_o	C_1	E_1 (meV)	C_2	E_2 (meV)
Single path (peak B)	3.83×10^8	18078±0.4	341.59±0.01	28.35±0.01		
Double path (peak B)	1.14×10^8	22208±3	70±610	16±65	12368±2	92±127
Single path (peak D)	7.25×10^6	6050±1	117.07±0.02	14.89±0.01		
Double path (peak D)	15649	7158±72	525±2	25±2	4±1	2.88±0.26

The origin of peak B (0.68 eV) is likely to be attributable to the transitions of free electrons near the bottom of the conduction band to a shallow acceptor level as suggested in Ref. 11. The lowest energy feature (peak A) about 70 meV below the shallow acceptor transition is also considered as Zn related emission since it has the similar characteristic with peak B in

temperature variation. An additional argument to support this is its PL emission being centered at 0.63 eV is very close to the region where the deep acceptor transition was observed for Mg doped InN. By comparing the results from previous experiment on Mg doped InN, the origins of the highest energy peak (peak D) can possibly be regarded as exciton features since its emission is centered at relatively high energy 0.72 eV and its linewidth broadening respect to temperature is related to the exciton-phonon interaction. Finally, the origin of peak C is likely a defect with low concentration as suggested in Ref. 3. Klochikhin *et al* explained that in the case of lower doping, the localized hole states of acceptor-type impurities and the tail states of the conduction band may play a noticeable role in the formation of interband luminescence [3].

4.2.3 Sample 656 (In-Rich)

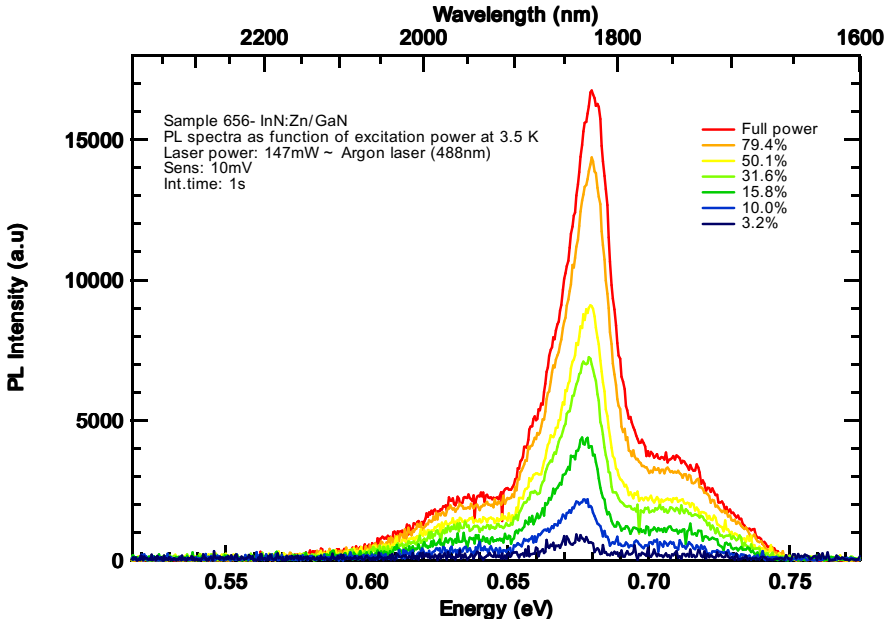

Figure 4.9 Variation of the PL spectrum of sample 656-InN:Zn with respect to excitation power at 3.5K. The spectrum was detected by an InSb detector with the 488nm line from an argon laser (150mW) as the excitation source.

Sample 656-InN:Zn was the first candidate to be grown under In-rich condition. As it mentioned briefly in the previous section, an In-rich condition might be preferable for efficient dopant incorporation into InN. By exploring different growth conditions, direct evidence of p-type luminescence is expected which will prompt a drive toward further interpretation of the optical properties of doped InN. A relatively high excitation power of 150mW was necessary to give detectable PL for this film. The PL spectra as a function of excitation power of sample 656-InN:Zn in figure 4.9 exhibits a strong and well shaped emission with indication of several emission peaks. The dominant peak is located at 0.68 eV

which is consistent with previous Zn doped InN (634-InN:Zn). Unfortunately, an unexpected absorption artifact near 0.65 eV disturbed the PL features and may effect the determination of the origin of the two lower energy peaks. In order to evaluate the details of the features, comprehensive multi peak fitting was done using the Igor software package. As demonstrated in figure 4.10, the structures are characterized by four stable features (peak A, B, C and D).

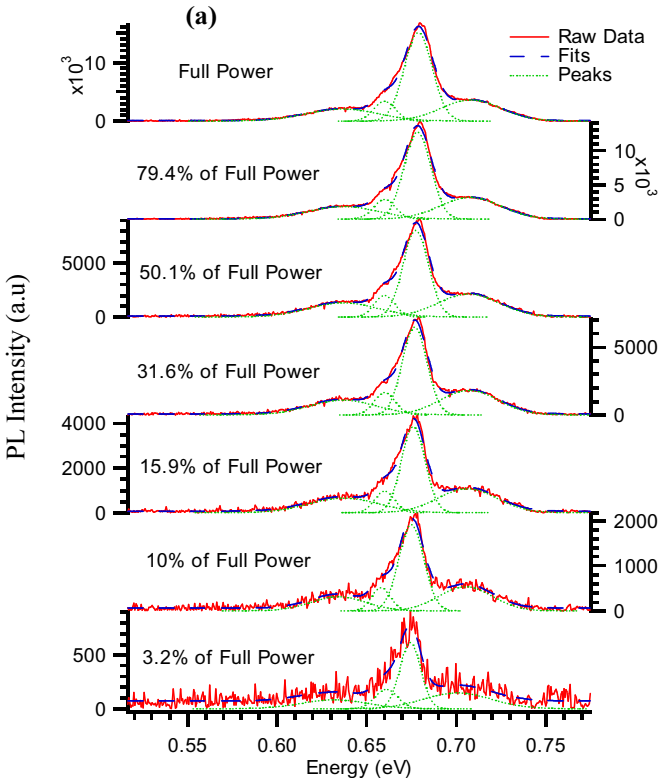

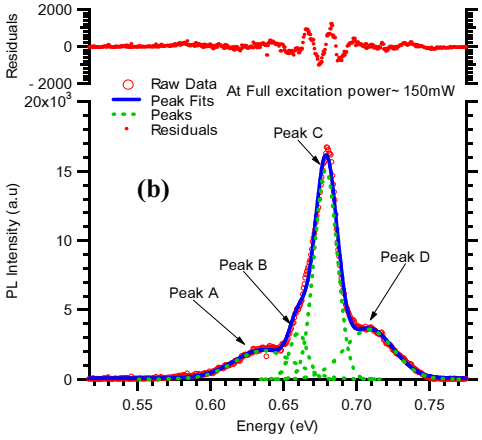

Figure 4.10 (a) PL spectra as a function of excitation power at 3.5K with multi peak fitting. (b) Demonstration of multi peak fitting with indication of four peaks (A, B, C and D)

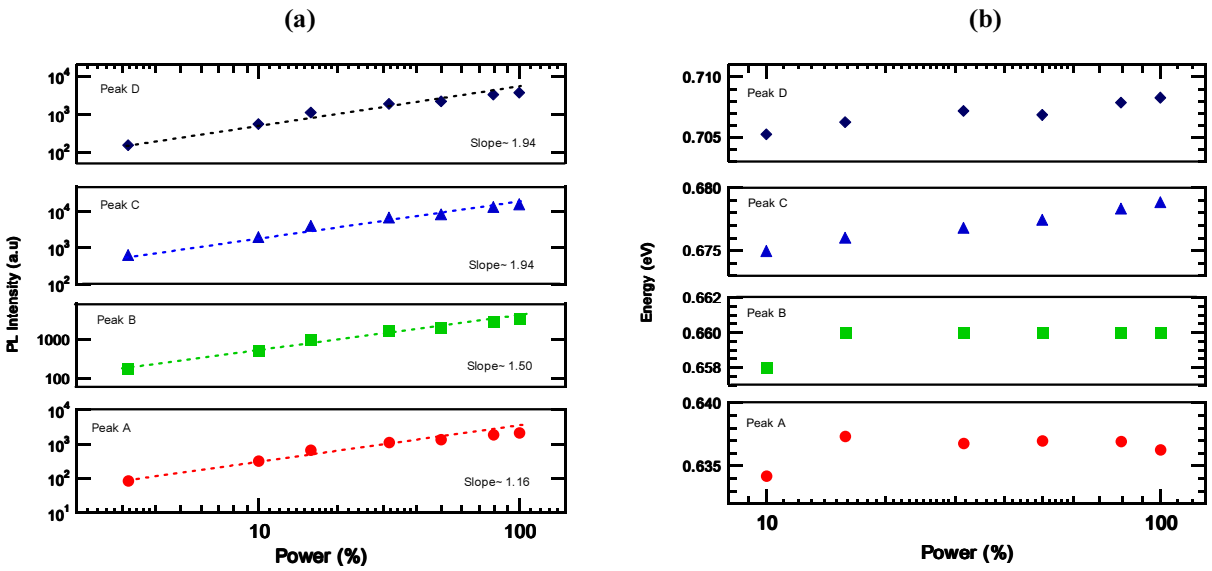

Figure 4.11 (a) Peak intensity and slope of straight line fit. (b) energy of peak A~D as a function of excitation power.

Furthermore, to evaluate the fundamental properties of each feature, normalized PL intensities and peak positions are depicted in figure 4.11 (a) and (b), respectively. It is clearly observed that the intensities of each peak gradually increase without any saturation as excitation power increase. The straight line fits for each plot yields below 2, indicating none of them are originated from band to band transition as pointed out in Ref 4.

The simultaneous peak energy fit in figure 4.11 explains that only two energy peaks shows the correlation regarding peak shifting as a function of excitation power. The PL emission peaks C (0.68eV) and D (0.72eV) exhibit blueshift approximately 4 meV as excitation power increases. In contrast, peak A (0.63eV) and B (0.66eV) exhibit no pronounced red or blue shift. The sudden drop of energy at the lowest excitation power for lower energy peaks may be influenced by the difficulty in defining the peak center due to relatively weak and noisy PL signal. Therefore it is sufficient to ignore the PL emission at 3.16% of full laser power and assumption that the peak energy is relatively stabilized with respect to excitation power.

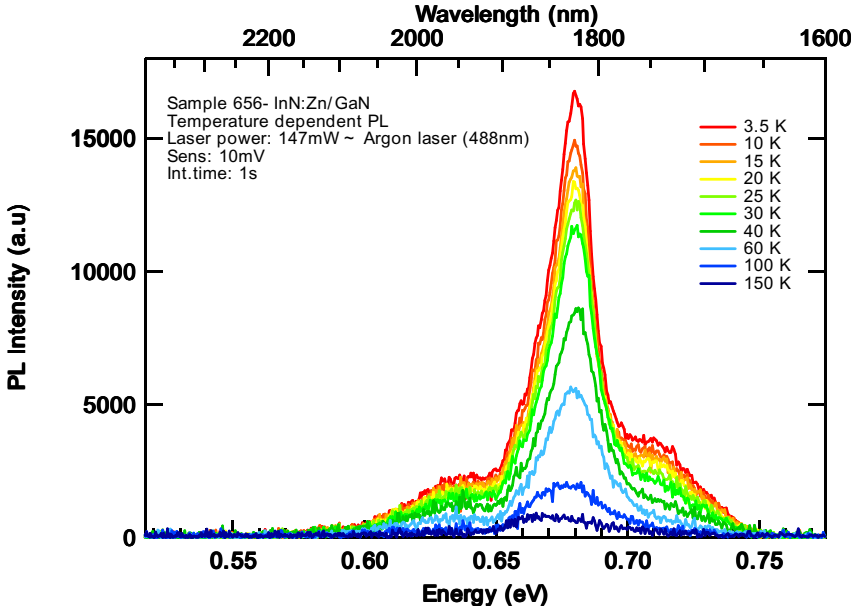

Figure 4.12 PL spectra for sample 656-InN:Zn as a function of temperature with constant excitation power (Argon laser ~147mW).

To further explore the nature of each peak, the PL spectra of sample 656-InN:Zn has been examined at various temperatures. Figure 4.12 shows the PL spectra recorded as a function of temperature with a constant excitation power. It is clearly observed that the PL intensity drastically depends on temperature with a typical redshift. The sensitivity of the PL spectrum to temperature shows that the population of one of two types of carriers forming the PL band

is strongly related to temperature [3]. Again, the data analysis software package Igor was used to peak fit individual lines to the spectra and the results of this fitting are presented in figure 4.13.

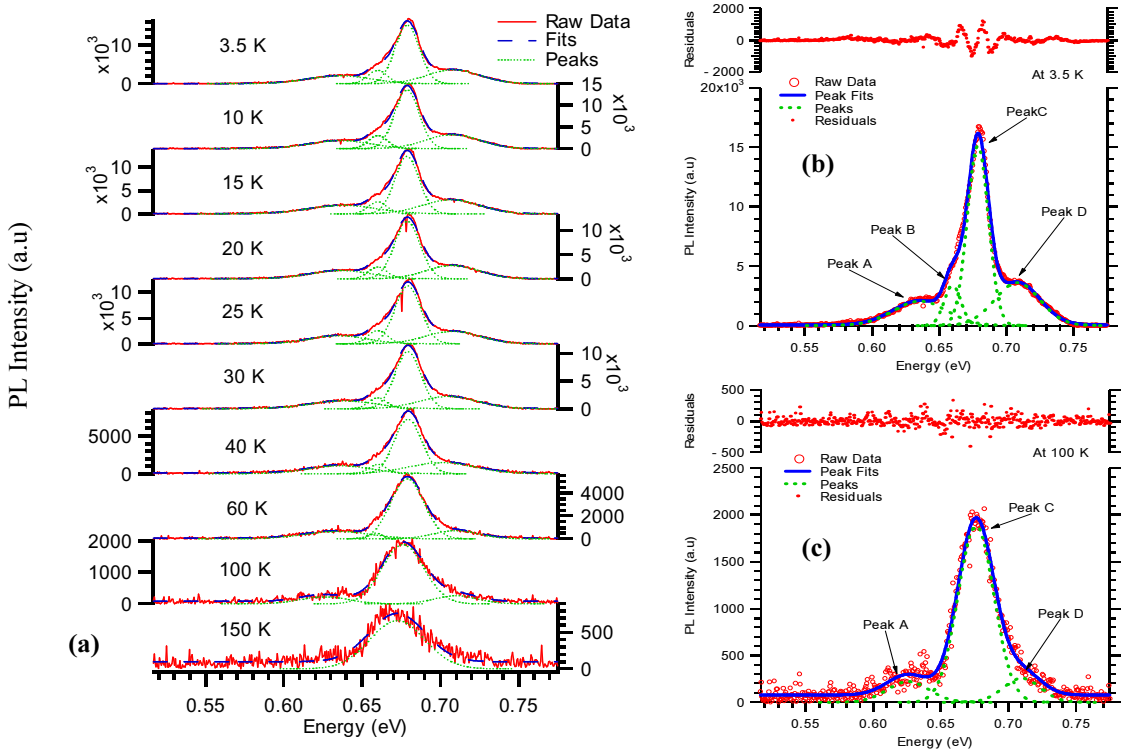

Figure 4.13 (a) The PL spectra as a function of temperature with multi peak fits. (b) Demonstration of the peak fitting at the lowest temperature ~ 3.5K. (c) Demonstration of the peak fitting at the highest temperature ~150K.

The noticeable change in temperature dependent PL is the absence of peak B (0.66 eV) at temperature above 80 K. The features A (0.63 eV) and B (0.66 eV) eventually merge as temperature increases which may ascribe to the effect of thermal ionization of electrons and holes in acceptor states. Furthermore, at the highest temperature ~150K only a single feature was detected as displayed in figure above. This phenomenon may be due to a considerable redshift and broadening as temperature rises which destroys the structure in the PL emission. However, each feature may still exist.

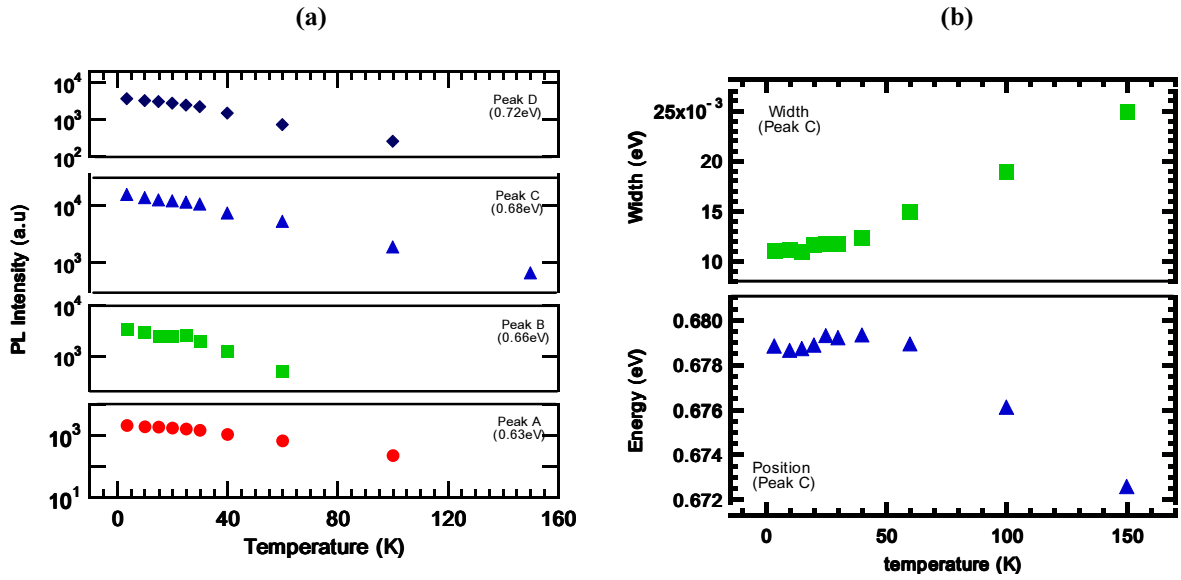

Figure 4.14 (a) Intensities of peak A, B, C and D as a function of temperature. (b) The energy and linewidth of dominant peak (peak C) in temperature dependent.

In order to clarify the nature of each peak, a plot of peak emission intensities as a function of temperature is displayed in figure 4.14 (a). The dominant energy emission peak (peak C ~0.68 eV) exhibits relatively strong variability compared to other peaks with temperature variations. Figure 4.14 (b) shows the energy and the linewidth of peak C as a function of temperature. The energy shift of the lines is due to the gap shrinkage effect in semiconductors that is caused by the cumulative effect of thermal lattice expansion and electron-phonon interaction [8]. It is interesting to notice that the peak shift as a function of temperature follow an 'S-shape' (decrease-increase-decrease). According to Ref. 10, the description that the thermal escape of carriers from lower energy localized states redistributes the carriers to higher energy localized states. The results of this, leads to the occurrence of an 'S-shaped' for temperature dependent peak positions as a function of temperature [9]. The linewidth of peak C (0.68 eV) increased about 25 meV from 4 K to 150 K. This result consists with the previous temperature dependent PL from sample 577-InN:Mg (figure 3.11 (b)). It is interesting to note that both PL emission peaks are centered at 0.68 eV.

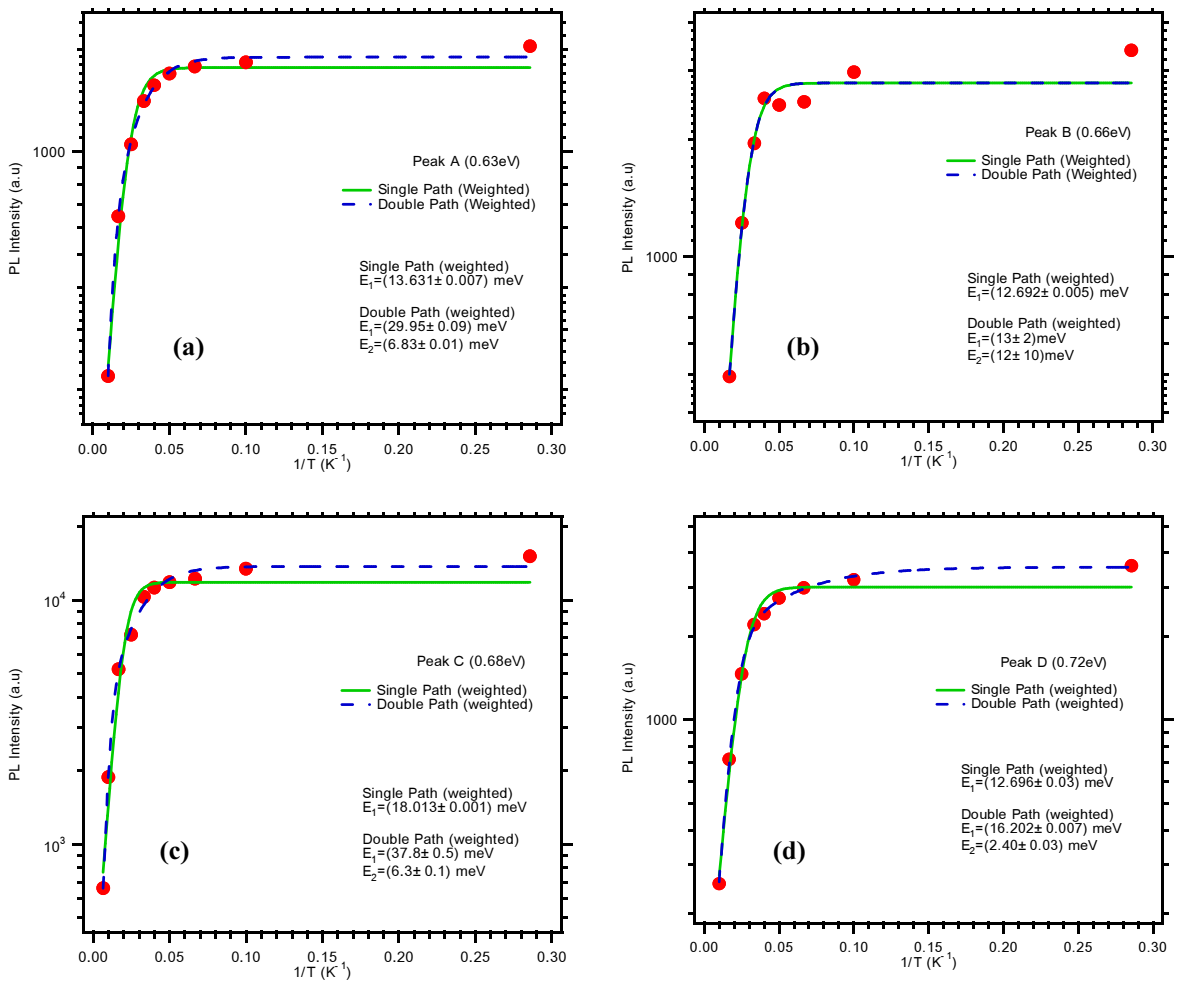

Figure 4.15 The Arrhenius plots of the PL emission intensities for (a) peak A (b) peak B (c) peak C (d) peak D

The Arrhenius plots showing single and double path activation energy fits for each feature are displayed in figure 4.15. Generally, as expected the two activation energy model gives a better fit than the single activation energy model. The single path weighted fit of each peak yield activation energies in a reasonable range between 12~18 meV. However, these values indicate the combination of the high and low temperature activation energies so it is difficult to deduce the origin of each process. Also the double path weighted fit has been examined. The results are thermal activation energies between 12~30 meV and 2~12meV for the high and low temperature ranges, respectively. The results show the disappearance of each peak is strongly associated with the activation energies in the high temperature region. The decay of each peak is in proportion to the value of activation energy E_1. For convenience, the parameters of each peaks and chi square values are displayed in table 4.3 where the coefficient C_1 and C_2 measure the strength of both quenching processes.

Table 4.3 Activation energy and Arrhenius parameters of sample 656-InN:Zn with single and double path weighted fit

	χ^2	I_o	C_1	E_1 (meV)	C_2	E_2 (meV)
Single path (peak A)	2.7×10^4	1764±1	31.69±0.03	13.63±0.01		
Double path (peak A)	3.8×10^4	1894±1	168±2	30±1	5.1±0.1	6.83±0.01
Single path (peak B)	7.0×10^5	2788.6±0.4	53.43±0.06	12.69±0.01		
Double path (peak B)	7.0×10^5	2790.2±0.5	70±260	13±2	13±264	12±10
Single path (peak C)	5.6×10^7	11815±1	58.02±0.01	18.01±0.01		
Double path (peak C)	5.6×10^7	11773±1	200±700	38±1	200±700	6.3±0.1
Single path (peak D)	8.7×10^5	3010.5±0.4	44.0±0.1	12.7±0.1		
Double path (peak D)	7.2×10^4	3548±1	76.74±0.07	16.21±0.01	1.3±0.6	2.4±0.1

According to the empirical investigation on doped InN and GaN, the origin of peak C is most likely to be attributable to the free electron transitions to the deep or shallow acceptor states. Reviewing from InN:Mg, the dominant peak (peak C) near energy of 0.68 eV is likely the emission from the shallow acceptor states [3]. Since, there is strong correlation between peak A (0.63 eV) and peak C (0.68 eV) in temperature variation as depicted in figure 4.14 (a), the origin of peak A also can be estimated as the free to bound transition. An addition argument supported by the similar PL feature from Ref. 10 and by comparing the PL emission from Mg doped InN, they suggested that the emission peak near energy of 0.63 eV is likely originated from deep acceptor states. The origin of B (0.66eV) can be regarded as a manifestation of structural disorder (crystal imperfection with shallow energy levels) [11] since there is no physical explanations to support its behaviour for both power and temperature dependent PL. Finally, the highest energy peak may be due to free exciton recombination as the energy emission peaks (D ~0.72eV) exhibits relatively weaker temperature variability compared to dominant peak (peak C). Also its binding energy (13~16 meV) is in good agreement with the fitting result of the activation energy from sample 634-InN:Zn (peak D ~15 meV).

4.3 References

[1] S. M. Durbin, C. E. Kendrick, C.H. Swartz, Y. W. Song, R. J. Reeves, J. Kennedy, Abstract for 7th Nitride Conference. Las Vegas, USA (2007).

[2] X. Wang, S.B. Che, Y. Ishitani and A. Yoshikawa, Appl. Phys. Lett. **90**, 201913 (2007)

[3] A. A. Klochikhin, V. Yu. Davydov, V. V. Emtsev, A. V. Sakharov, and V. A. Kapitonov, Physical Review B **71**, 195207 (2005)

[4] F. Chen, A. N. Cartwright, H. Lu, and W. J. Schaff, Physica E **20**, 308 (2004)

[5] C. Hsiao, H. Hsu, L. Chen, C. Wu, C. Chen, M. Chen, L. Tu and K, Chen, Appl. Phys. Lett. **91**, 181912 (2007)

[6] N. Khan, N. Nepal, A. Sedhain, J. Y. Lin, and H. X. Jiang, Appl. Phys. Lett. **91**, 012101 (2007)

[7] G. W. Shu, P. F. Wu, M. H. Lo, J. L. Shen, T. Y. Lin, H. J. Chang, Y. F. Chen, C. F. Shih, C. A. Chang, and N. C. Chen, Appl. Phys. Lett. **89**, 131913 (2006)

[8] C. Boemare, T. Monteiro, M.J. Soares, J. G. Guilherme and E. Alves. Physica **B** 308-310 (2001) 985-988

[9] Q. Li, S. J. Xu, M. H. Xie and S. Y. Tong. J. Phys: Condens. Matter **17** (2005) 4853-4858

[10] B. Arnaudov, T. Paskova, P. P. Paskov, B. Magusson, E. Valcheva, and B. Monemar, H. Lu, W. J. Schaff, H. Amano and I. Akasaki, Phys Review B **69**, 115216 (2004)

[11] S. Z. Wang, S. F. Yoon, Y. X. Xia and S. W. Xie, Journal of Appl Phys Vol **95** No. 12

Chapter 5 Conclusion and Future Research

5.1 Summary of Results

There is plausible evidence to show Mg and Zn are viable p-type dopants for InN from the photoluminescence result. The demonstration of the PL emission from doped InN provides considerable motivation that p-type InN could be used for the eventual fabrication of pn junction devices in the future. However, it is yet to be established that the vital aspects of p-type InN are fully understood. Evaluating the fundamental properties of p-type luminescence remains a formidable challenge due to the difficulty in producing high quality films. The optical properties of Mg and Zn doped InN are still somewhat obscured by conflicting arguments regarding the origin of the observed transitions.

The Mg doped InN was grown on YSZ substrates by molecular beam epitaxy (MBE). A series of Mg doped InN films, grown at different Mg cell temperatures range from 170 to 370 ˚C were characterized by PL. To investigate the Mg dopability of InN, a series of InN:Mg samples have been analyzed by SIMS (secondary ion mass spectroscopy) and Mg concentrations in InN films were estimated. The general aim of this research was focused on the light emitting processes for p-type InN and its fundamental properties. The correlation between the effect of the Mg concentration and optical properties of Mg doped InN was also comprehensively investigated. The PL measurement was performed by two different lasers (diode and argon) as excitation sources and the “Minimate” spectrometer was coupled with an InSb detector for analysis of the spectra. Hall measurements revealed n type conductivity for the all of the Mg doped InN films. Due to electron accumulation layers on its surface, it is difficult to electrically measure p-type InN.

The first impression of PL response from Mg doped InN was detected from the films with T_{Mg}=225 ˚C, Mg_{conc}= 8.7×10^{17} cm^{-3}(555-InN:Mg). It is interesting to notice that the dominant peak emission is centered near 0.6 eV. Compared to PL emission of unintentionally doped InN

(~0.7 eV), the dominant peak is redshifted approximately 0.1 eV. Subsequently, PL performance for a series of Mg doped InN films was studied by taking 555-InN:Mg as a reference. PL is observed with significant intensity from the samples grown with T_{Mg} from 170 ˚C to 230 ˚C.

It is found that there are strong correlations between dominant emission peaks and Mg cell temperatures. Perhaps the most striking observation of the PL results is the dominant peaks at two different energies (near 0.6 eV and 0.68 eV) depending on T_{Mg}. The films with high Mg concentration (555, 585, 590-InN:Mg) had maximum emission near 0.6 eV. Meanwhile, the emission PL peaks of the films with low Mg content are centered at 0.68 eV. This result indicates the PL spectral peak positions of InN:Mg samples are significantly affected by Mg concentration. Further, no PL emission was observed from the films with T_{Mg} above 230 ˚C. Eventually, to explore the relation between the PL intensities and T_{Mg}, the PL emissions from samples with a peak near energies of 0.68 eV were examined closely. Thus it was found that samples grown with low T_{Mg} yield relatively high PL intensities. According to the empirical investigation on Mg doped GaN, whether they revealed as p-type or n-type, Mg was distinctly making GaN semi-insulating. Considering the many similarities between InN and GaN, the origin of dominant PL peaks for Mg-doped InN may be luminescence from deep and shallow acceptors (free to bound).

The structure of the PL spectra of Mg doped InN samples are the manifestation of various optical transitions. The PL features were characterized by excitation intensity and temperature variations. In order to evaluate the details of the features, the data analysis software package IGOR was used to peak fit individual lines to the spectra. The data fitting process returned PL line parameters such as position, intensity and linewidth. The prominent blue shift is pronounced in PL spectra as a function of excitation power. There are different types of physical explanations which apply for each free to bound and donor acceptor pair transitions. The shift of a free to bound transition is mainly influenced by the band filling effect in the conduction band. Meanwhile, the prominent shift for donor acceptor pair transitions is associated with the Coulomb interaction. A typical redshift is mainly observed from free to bound transitions as a function of temperature. This is ascribed as the band shrinkage as temperature rises. Finally, many aspects of luminescence mechanisms are evaluated by empirical Varshni’s equation for bandgap determination and Arrhenius fits for the thermal activation energies for each transition. The activation energies for free to bound transitions are

in the range between 15~20 meV, indicating the positions of deep and shallow acceptor levels above the valence band.

5.2 Future Prospect of P-type InN

The great success in determining Mg as a suitable dopant for InN provides motivation for further investigation into p-type InN. In considering the similarity between InN and InAs, Zn is introduced as a potential candidate for a viable p-type dopant of InN. The PL features from Zn doped InN also resemble the results from Mg doped InN and the descriptions of observed transitions are defined in similar manners. It is also found that growing samples in In-rich conditions (InN:Zn) gives a PL signal which is significantly improved. For the completeness of the analysis, PL from InN:Zn films have also been characterized by the Igor software package and their properties were studied. The energy of the observed PL emission peaks from InN:Mg and InN:Zn films are compared and displayed in figure 5.1. Both dopants give prominent emissions from transitions of free electrons near the bottom of the conduction band to two acceptor levels: shallow and deep. It is worth noting that the observed shallow acceptor transitions are commonly presented at an energy of 0.68 eV (no indication of shallow acceptors in high Mg concentration InN) and deep acceptors are presented between 0.6 and 0.63 eV for both Zn and Mg dopants.

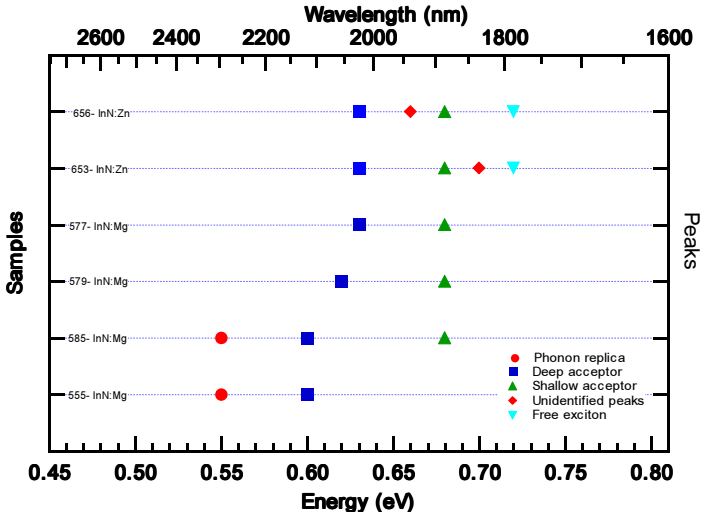

Figure 5.1 The observed emission from characterized samples (with significantly large PL signals). The symbols indicate the origin of different transitions. The emissions between 0.6~0.63 eV are likely to be the deep acceptor transition. Meanwhile observed transitions at the energy of 0.68 eV originated from shallow acceptor. The emissions at the highest energy of 0.72 eV are most likely the free exciton features.

Improved film quality of InN:Zn samples resulted in PL emissions with more structures than observed in the PL of InN:Mg. These results motivate towards future investigation into p-type luminescence mechanisms for InN. Perhaps, the prominent results from Zn may lead to significant steps towards feasible InN based pn junction devices.

In order to evaluate the properties of p-type luminescence mechanisms, a different combination of spectrometer and detector is also suggested to improve the PL detection. In the last month of research a new spectrometer, "Acton", and an InGaAs detector were purchased to detect the PL from heavily Mg and Zn doped samples. Surprisingly, the new application improved the detected PL signal by about 250 times compared to the combination of "Minimate" and InSb detector. Prominent PL features as shown in figure 5.2, were detected from the samples which failed to exhibit any detectable PL in the previous investigation.

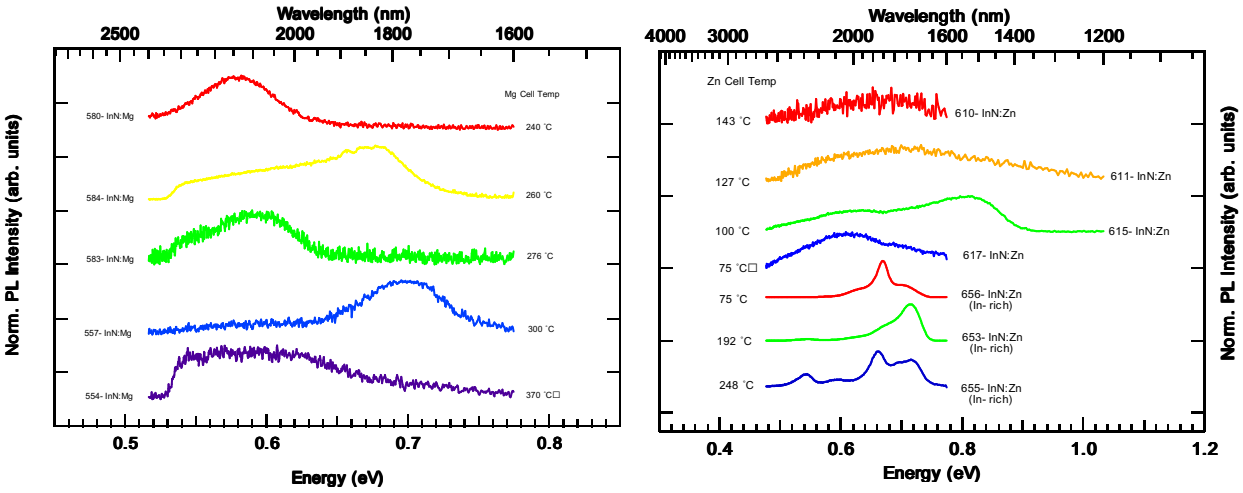

Figure 5.2 (a) PL spectra obtained with the combination of Acton spectrometer and InGaAs detector for samples with T_{Mg} higher than 240 ˚C. (b) PL spectra with combination of Acton spectrometer and InSb detector for samples with T_{Zn} higher than 127 ˚C.

Despite lack of significant PL signal from heavily doped samples, PL from heavily doped samples is worthwhile to explore, showing the fact that p-type InN is capable of light emission. The optical properties of p-type luminescence are still not fully understood, but the growth and characterization are developing at a remarkable rate.